On the coarse-graining of polymers into bead-spring chains

Patrick T. Underhill, Patrick S. Doyle*

Department of Chemical Engineering, Massachusetts Institute of Technology, Cambridge, MA 02139, USA

Abstract

We present a study of the coarse-graining of polymers into bead-spring chains using statistical mechanics. The force–extension behavior is examined at different levels of coarse-graining. A direct result of the springs being decoupled is that the force–extension behavior depends only on the number of flexibility lengths (e.g. persistence or Kuhn lengths) represented by each spring. This dimensionless parameter is found to govern the fluctuations around the mean extension, analogous to the conventional role of temperature. The use of an effective flexibility length to correct the model behavior is analyzed, and we have calculated bounds on the choices of this correction factor. The analytic nature of the statistical mechanical framework has also allowed for the calculation of asymptotic and universal behavior. The zero Weissenberg number rheological behavior is examined using the retarded-motion expansion coefficients of bead-spring chains at different levels of coarse-graining. The results show the trade-off between using too few or too many springs. The general framework to analyze the force–extension and rheological behavior is applied to the worm-like chain, FENE, and Fraenkel models. We introduce a new method for coarse-graining a polymer into a bead-spring chain called the Polymer Ensemble Transformation (PET) method. Application to the freely jointed chain polymer yields a set of spring force-laws called the Random Walk Spring (RWS) model. This new method illustrates why the previous spring force-laws cannot be used to finely discretize polymers and also provides new insight into how to rationally proceed in the coarse-graining of polymers into bead-spring chains.
© 2004 Elsevier B.V. All rights reserved.

Keywords: Coarse-graining; Bead-spring models; Statistical mechanics

1. Introduction

Polymers are challenging to model due to the wide range of time and length scales in the system. A recurring theme in the development of polymer models and simulations is the idea of coarse-graining. The goal in coarse-graining is to produce a model that has reduced complexity such that it is tractable to calculate the properties of the model while simultaneously capturing molecular properties to sufficient accuracy.

Some of the earliest attempts at coarse-graining polymers consisted of eliminating degrees of freedom for which there are only small fluctuations, such as bond lengths and bond angles. This led to models including the freely jointed chain (FJC) in which each bond is treated as a free joint and the freely rotating chain (FRC) [1]. A much more successful model which includes hindered rotation is the

rotational isomeric state (RIS) model [2]. While RIS has been successful in determining the equilibrium properties of polymers, understanding the dynamics of polymers requires the use of a coarser model.

One example of a coarser model is a FJC in which the length of a step is taken to be larger than a bond [3]. In this model the length of a rod, or Kuhn length, represents the length over which the polymer acts as if the steps were uncorrelated. This model represents a chain that is coarse-grained to the length of a Kuhn length. One great advantage of this model is that the distribution function of configurations is well-known from the theory of random walks. It should be noted that there is a difference between the random walk distribution and the bead-rod chain with *rigid* constraints [4]. This latter model with rigid constraints will be referred to solely as the Kramers chain in this paper. The former model, with a distribution function identical to the random walk, will be referred to as either the freely jointed chain or random walk chain.

---

* Corresponding author.
E-mail address: pdoyle@mit.edu (P.S. Doyle).

Using this knowledge of the distribution function it has been shown that the FJC has an elastic restoring force that is linear for small deformations, and is given by the inverse Langevin function over the entire range of deformations [3]. Although other polymer models, such as the worm-like chain (WLC), have a different form for the restoring force, this elasticity is one of the main properties of polymers that distinguishes them from small molecules and thus must be captured in a coarse-grained model. The restoring force is primarily due to the entropy of the polymer so it is often referred to as the "entropic restoring force". When developing a coarse-grained polymer model, the fine details of the polymer configurations must necessarily be lost. These "microstates" contribute significantly to the entropy, and thus to the elastic restoring force. Something else must be added to the system that represents this restoring force without representing all the "microstates". This restoring force has often been represented by springs, thus modelling the polymer as a bead-spring chain.

While much work has been performed using Hookean springs, it is well known that finite-extensibility plays an important role in determining the rheological properties of polymers [4–7]. For that reason, this paper will focus primarily on springs that have a finite fully extended length. However, within this class of springs, there exists a wide variety of forms for the spring force-law [8]. These include the worm-like chain model [9,10], the finitely extensible nonlinear elastic (FENE) model [11], and other approximations to the inverse Langevin function [12]. Note that in this paper we do not consider any of the numerous closure approximations that have been proposed in the literature [5,13]. Furthermore, for each of the models there are discrepancies in the literature as to the "best" parameters that should be chosen for the spring force-law in order to have an accurate representation of the polymer behavior [14–16].

Most of these previous studies have used Brownian dynamics to examine the rheological properties of the chains, and then used some procedure to determine the parameters in the model. In fact only a few studies have looked explicitly at the force–extension behavior of bead-spring chains. Larson et al. [17,18] showed using Brownian dynamics that the force–extension behavior of a bead-spring chain changes as more and more beads are added to the chain. They found that a parameter in the force-law (the persistence length for the case of the WLC model) could be *artificially changed* to obtain better results from the model. However, no guidelines have been given for the use of such a method. Furthermore, the conditions under which the method fails have not been quantified, and the consequences of the artificial change have not been evaluated. For these reasons, there has been variability between investigators as to the best way to implement the correction, or even *if* the correction should be used. To answer important questions *including but not limited to* these, one must analyze in a systematic way the ramifications of coarse-graining a polymer into bead-spring chains.

Understanding the behavior of bead-spring chains, in particular under what conditions they represent accurate coarse-grained models, is becoming increasingly important in the study of polymers. Previous studies have suggested that bead-spring chains only accurately represent polymers when each spring represents a large segment of polymer. The study by Larson et al. suggests that springs can only model the WLC if each spring represents a large number of persistence lengths. Similarly, Somasi et al. [14] have argued based on the force–extension behavior of the Kramers chain [19] that springs can only represent a Kramers chain if each spring represents more than 10 Kuhn lengths. Thus from force–extension behavior it would seem that a single spring (or dumbbell) model would best represent a polymer.

However, some rheological considerations require the opposite extreme, that the polymer is modelled by as many springs as computationally tractable. The behavior of a polymer in flow is highly dependent on the drag exerted on the polymer by the solvent. In a bead-spring chain model, the drag is exerted on the chain only at the beads. Thus the drag will only be exerted along a continuous contour in the limit of a large number of springs. The rheological behavior of a polymer is also dependent on its distribution of relaxation times. To capture this distribution, the bead-spring model must have a large number of modes, and thus a large number of springs [4]. Finally, the large number of springs may be motivated primarily by geometry. If a polymer is placed in a confining geometry, its behavior can only be described correctly if the model represents the polymer at a small enough length scale [20–22]. The task of modelling a polymer accurately using bead-spring chains is one of balancing these two opposing considerations. The number of springs must be *simultaneously* large enough and small enough.

The force–extension behavior is of fundamental importance to the understanding of bead-spring chains and the choice of force-law. The very idea of replacing the polymer by springs is motivated by the force–extension behavior of the polymer. Thus we begin our systematic study of bead-spring chains by analyzing their force–extension behavior. While other investigators have used Brownian dynamics to look at the force–extension behavior, we use both Brownian dynamics and equilibrium statistical mechanics. Although the methods give *identical* results, equilibrium statistical mechanics has major advantages. The statistical mechanical analysis avoids the stochastic noise intrinsic in Brownian dynamics simulations so the force–extension behavior can be calculated quickly and accurately. The analytic nature also allows for the easy identification of the important dimensionless parameters, as well as the construction of series expansions when those parameters become either large or small.

After understanding the force–extension behavior we can turn to the study of rheological properties, applying what has been learned. The first step from force–extension behavior to rheology is examining zero Weissenberg number rheology.

This is because in zero Weissenberg number flow, a polymer has sufficient time to sample all of phase space. To examine this limit, the retarded-motion expansion coefficients of the bead-spring chain can be examined.

This paper is organized as follows. In Section 2 the two methods used, equilibrium statistical mechanics and Brownian dynamics, are reviewed briefly. Section 3 contains an extensive analysis of the force–extension behavior of the bead-spring chains. This includes a discussion of the correction-factor employed by Larson et al. [18], a discussion of the fluctuations about the mean extension, and a discussion of universal behavior. Section 4 examines the rheological behavior of the bead-spring chains in the limit of zero Weissenberg number by examining the first two coefficients of the retarded-motion expansion. In Section 5 the analysis in the previous sections is shown to be generally valid for any choice of force-law by showing explicitly how the analysis would be performed for two other important models. The two examples given are the FENE force-law and the infinitely stiff Fraenkel force-law (equivalent to the FJC). Section 6 introduces a new method for choosing the spring force-law called the Polymer Ensemble Transformation (PET) method. We apply this method to the FJC to calculate a spring force that *exactly* matches the force–extension behavior of the FJC called the Random Walk Spring (RWS) model. Not only does this new model perform better than the previous models, the method illustrates *why* the other models perform in the manner discussed throughout the earlier sections.

2. Methodology

The behavior of bead-spring chains at different levels of coarse-graining has been investigated using two methods that will be reviewed briefly here, statistical mechanics and Brownian dynamics.

2.1. Statistical mechanics

In this paper we will only be discussing systems for which equilibrium statistical mechanics can be applied. Within this context of equilibrium statistical mechanics the probability density of a configuration is proportional to [23]

$$\exp\left[\frac{-\mathcal{H}_{\text{eff}}}{k_B T}\right] \tag{1}$$

if the configuration is consistent with the macroscopic constraints. The quantity $\mathcal{H}_{\text{eff}}$ is the effective Hamiltonian, k_B is Boltzmann's constant, and T is the absolute temperature. The specific form of the effective Hamiltonian depends on the macroscopic constraints, i.e. the ensemble. For the often used canonical ensemble the effective Hamiltonian is equal to the energy.

Given the above definition, the probability density at the configuration i, p_i, is given by

$$p_i = \frac{1}{\mathcal{Z}} \exp\left[\frac{-\mathcal{H}_{\text{eff},i}}{k_B T}\right] \tag{2}$$

where $\mathcal{Z}$ is the partition function and is equal to

$$\mathcal{Z} = \underset{\{\text{configurations}\}}{\int \cdots \int} \exp\left[\frac{-\mathcal{H}_{\text{eff}}}{k_B T}\right] d\mathbb{V} \tag{3}$$

to ensure that the probability density is properly normalized. It should be noted that for the bead-spring chains considered in this paper we do not need to worry about the kinetic energy contribution to the effective Hamiltonian and the momentum configuration space [4]. This is because our system has no rigid constraints that freeze-out degrees of freedom, and also we will not compute the average of any quantity that depends on momentum.

Average quantities are computed by integrating that quantity times the probability density over all the configuration space. Thus for a property signified by $\mathcal{F}$ the average is

$$\langle \mathcal{F} \rangle = \underset{\{\text{configurations}\}}{\int \cdots \int} \mathcal{F} \frac{1}{\mathcal{Z}} \exp\left[\frac{-\mathcal{H}_{\text{eff}}}{k_B T}\right] d\mathbb{V} \tag{4}$$

2.2. Brownian dynamics

The technique of Brownian dynamics (BD) [24,25] has been widely used to study the non-equilibrium and equilibrium properties of polymer models in flow, in particular bead-rod and bead-spring models [19,26,27]. Most previous investigations of the behavior of bead-spring chains have used BD. Because the systems studied in this paper can all be analyzed using equilibrium statistical mechanics also, we find it natural to use that methodology. In order to provide an explicit link between the statistical mechanical results and previous work using BD, we will perform BD simulations of the force–extension behavior of the bead-spring chains. This will verify that the two methods give *identical* results.

The method of BD consists of integrating forward in time the equation of motion for each of the beads in the polymer. The equation of motion is given by

$$m_i \ddot{\mathbf{r}}_i = \mathbf{F}_{\text{net},i} = \mathbf{F}_{B,i} + \mathbf{F}_{d,i} + \mathbf{F}_{s,i} \simeq \mathbf{0} \tag{5}$$

where the subscript i denotes bead i, m the mass of each bead, $\ddot{\mathbf{r}}$ the acceleration, $\mathbf{F}_{\text{net}}$ the net force, $\mathbf{F}_B$ the Brownian force due to collisions of the solvent molecules with the beads, $\mathbf{F}_d$ the drag force due to the movement of each bead through the viscous solvent, and $\mathbf{F}_s$ the systematic force on each bead due to the springs and any external forces. The drag on each bead is taken to be the Stokesian drag on a sphere, and we will neglect any hydrodynamic interaction between beads. Thus,

$$\mathbf{F}_{d,i} \simeq -\zeta \left(\dot{\mathbf{r}}_i - \mathbf{u}^\infty(\mathbf{r}_i) \right) \tag{6}$$

where ζ is the drag coefficient, and $\mathbf{u}^\infty(\mathbf{r}_i)$ is the undisturbed solvent velocity evaluated at the center of bead i. The governing stochastic differential equation then becomes

$$\dot{\mathbf{r}}_i(t) \simeq \mathbf{u}^\infty(\mathbf{r}_i(t)) + \frac{1}{\zeta}[\mathbf{F}_{s,i}(\{\mathbf{r}_j(t)\}) + \mathbf{F}_{B,i}(t)] \qquad (7)$$

The Brownian force is chosen from a random distribution such that it has the following expectation values:

$$\langle \mathbf{F}_{B,i}(t) \rangle = \mathbf{0} \qquad (8)$$

$$\langle \mathbf{F}_{B,i}(t)\mathbf{F}_{B,j}(t) \rangle = \frac{2k_B T\zeta\delta_{ij}}{\delta t}\boldsymbol{\delta} \qquad (9)$$

The symbol δ_{ij} is the Kronecker delta, $\boldsymbol{\delta}$ the unit second-order tensor, and δt the time-step. These expectation values are needed so that the system satisfies the fluctuation-dissipation theorem. The stochastic differential equation can be re-written as

$$\dot{\mathbf{r}}_i(t) \simeq \mathbf{u}^\infty(\mathbf{r}_i(t)) + \frac{1}{\zeta}\mathbf{F}_{s,i}(\{\mathbf{r}_j(t)\}) + \sqrt{\frac{2k_B T}{\zeta\,\delta t}}\,\mathrm{d}\mathbf{W}_i \qquad (10)$$

where $\mathbf{W}_i$ is a Wiener process that satisfies

$$\langle \mathrm{d}\mathbf{W}_i \rangle = \mathbf{0} \qquad (11)$$

$$\langle \mathrm{d}\mathbf{W}_i\,\mathrm{d}\mathbf{W}_j \rangle = \delta_{ij}\,\boldsymbol{\delta} \qquad (12)$$

In the work presented here we will use a simple explicit first-order time-stepping algorithm:

$$\mathbf{r}_i(t + \delta t) \simeq \mathbf{r}_i(t) + \dot{\mathbf{r}}_i(t)\,\delta t \qquad (13)$$

It should be noted that when simulating bead-spring chains with finitely extensible springs with the above criteria for the Brownian force and an explicit time-stepping scheme, there can be a small but finite probability that the Brownian force will cause a spring to be stretched beyond the fully extended length. In the simulations presented in this paper, the time-step δt was always taken small enough such that no examples of over-stretching were observed over the course of the simulation time.

In the BD simulation performed of the force–extension behavior, the system was equilibrated for

$$t_{eq} = 4 \times 10^3 \left(\frac{\zeta A_{true}^2}{k_B T}\right) \qquad (14)$$

where A_{true} is the true persistence length of the polymer. The z-position of the end of the bead-spring chain was then averaged for

$$t_{ave} = 8 \times 10^3 \left(\frac{\zeta A_{true}^2}{k_B T}\right) \qquad (15)$$

The time-step used was

$$\delta t = 4 \times 10^{-3} \left(\frac{\zeta A_{true}}{f}\right) \qquad (16)$$

where f is the externally applied force. Variance reduction [24] was also employed to reduce the stochastic noise at small force.

3. Force–extension behavior

As was mentioned in the introduction, one of the most important and widely known properties of polymers is elasticity, and in particular the presence of an "entropic restoring force". Furthermore, with the advent of optical and magnetic tweezer technologies, much more attention is being paid to the relation between force and extension [28]. In particular, these experiments have been used to test polymer models which are then used in other contexts. *Making quantitative calculations of the force–extension behavior of bead-spring chains for comparison with the polymers they represent is the goal of this section.*

3.1. System definition

The typical set-up used to calculate the restoring force using statistical mechanics is shown in Fig. 1. One end of the polymer is tethered at the origin, and a constant external force, f, is applied to the other end of the polymer. The direction of this constant force defines the z-direction of the coordinate system. The x and y coordinates are therefore in the plane perpendicular to the applied force. The expectation value of the polymer's z displacement, $\langle z \rangle$, can be calculated as a function of the applied force. This function, $\langle z \rangle$ vs. f, defines the polymer's force–extension (F–E) behavior. Note that this is different from the behavior found by performing the analysis shown in Fig. 2, in which the ends of the polymer are held fixed at points that are z (or equivalently r) distance apart and the average force, $\langle f \rangle$, to hold them at those positions is calculated. Because the former approach is more computationally tractable than the latter, it has been the preferred approach by previous investigators using bead-spring chains, and it will be the approach initially used here. See Section 6 for a more detailed comparison of the two approaches.
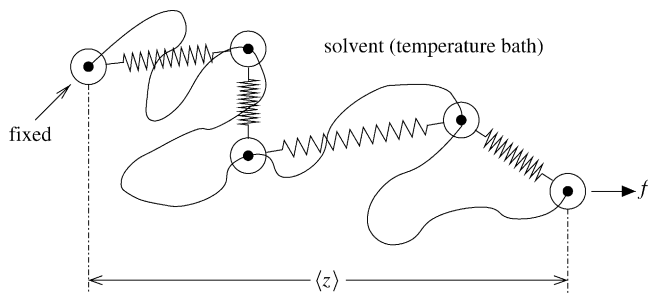

Fig. 1. Illustration of a polymer and bead-spring model in the constant force ensemble. One end is held fixed, while a constant force is applied to the free end. The direction of the force defines the z-direction. The z-displacement of the chain is averaged.
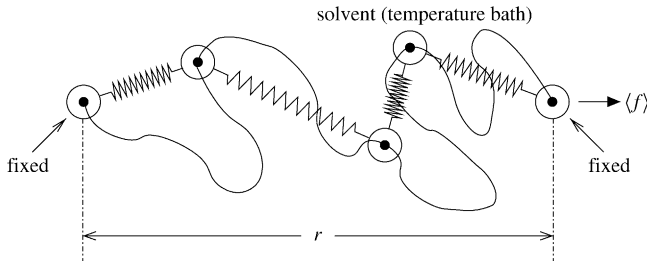
Fig. 2. Illustration of a polymer and bead-spring model in the constant extension ensemble. Both ends are held fixed at a distance r apart. The external force required to hold one of the ends fixed is averaged.

When developing a bead-spring model for the polymer, it is crucial to verify that the model accurately describes the polymer. Because the concept of replacing the polymer by a bead-spring chain is largely motivated by the F–E behavior, it seems natural to verify the accuracy of the coarse-graining by requiring that the F–E behavior of the bead-spring chain is the same as the polymer it represents. However, it is also critical that the bead-spring chain is compared to the polymer using the exact same "experiment". Since the polymer behavior is calculated by applying a constant force, as shown in Fig. 1, the bead-spring behavior will be calculated in the same way.

3.2. Decoupled springs

Because the bead-spring model is in the $(N_p)fT$ ensemble (the number of polymers N_p is trivially held constant at one), the effective Hamiltonian is obtained by performing a Legendre Transform from z to f [23]. Thus the effective Hamiltonian is

$$\mathcal{H}_{\text{eff}} = U - fz_{\text{tot}} \tag{17}$$

where U is the potential energy of the bead-spring system (recall that all kinetic energy has been dropped), and z_{tot} the z-coordinate of the end of the chain. For all the systems considered here, the potential energy will have no bending potentials, and the energy for each spring will only depend on the magnitude of extension. It should then be clear that the effective Hamiltonian can be separated into a sum over each spring

$$\mathcal{H}_{\text{eff}} = \sum_j [U_s(r_j) - fz_j] \tag{18}$$

where j denotes each spring, $U_s(r_j)$ the potential energy of each spring as a function of the radial extension of the spring, and z_j the z-displacement of spring j. Because the effective Hamiltonian can be decomposed into a sum over each spring, the partition function for the whole chain, $\mathcal{Z}_w$, splits into a product of the partition functions for single springs, $\mathcal{Z}_s$,

$$\mathcal{Z}_w = (\mathcal{Z}_s)^{N_s} \tag{19}$$

where N_s is the number of springs in the chain, and $\mathcal{Z}_s$ is given by

$$\mathcal{Z}_s = \int \exp\left[\frac{-U_s(r) + fz}{k_B T}\right] d^3r \tag{20}$$

This separation of the partition function has two important consequences. First, the computational effort needed to calculate the F–E behavior is greatly reduced because the properties of any size chain can be determined by knowing the properties of a *single spring* (a single integral). Second, it illustrates that for this set of conditions the springs are decoupled. In particular, it will be shown later that the F–E behavior of these bead-spring chain models does not depend explicitly on the number of beads, which act as free hinges, but only depends on the level of coarse-graining for each spring. This is counter to other investigators who have argued the importance of the number of springs in the bead-spring chain model [18].

3.3. Dimensionless parameters

In describing the behavior of bead-spring chains it is useful to define a set of dimensionless variables. Many of these variable transformations are motivated by the worm-like chain (WLC) force-law, which is the force-law that correctly describes the behavior of dsDNA. Specifically the transformations are motivated by the interpolation formula approximation to the WLC by Marko and Siggia [10]. However, it must be noted that the formula remain general, as will be shown later in Section 5. A summary of these parameters and their physical interpretations is given in Table 1. These dimensionless variables are

$$\hat{z}_{\text{tot}} \equiv \frac{z_{\text{tot}}}{L}, \qquad \hat{r} \equiv \frac{r}{\ell}, \qquad \hat{f} \equiv \frac{fA_{\text{true}}}{k_B T}, \qquad \alpha \equiv \frac{L}{A_{\text{true}}},$$

$$\lambda \equiv \frac{A_{\text{eff}}}{A_{\text{true}}}, \qquad \nu \equiv \frac{\alpha}{N_s} = \frac{\ell}{A_{\text{true}}} \tag{21}$$

where L is the contour length of the chain, $\ell \equiv L/N_s$ the fully extended length of a spring, A_{true} the true persistence length of the polymer, α the number of true persistence lengths in the polymer's contour, A_{eff} the effective persistence length, λ the ratio of the effective persistence length to the true persistence length, and ν the number of true persistence lengths represented by each spring. It is also useful to define two energy functions. First, we will denote as $U_{\text{eff}}(r)$ the spring potential, $U_s(r)$, with all additive constants dropped. This is done as a convenience and changes no results. Second, a dimensionless energy is defined as

$$\hat{U}_{\text{eff}}(\hat{r}) = \frac{U_{\text{eff}}(r)}{k_B T} \frac{\lambda}{\nu} \tag{22}$$

It will become clear later that this scaling is the one appropriate for the spring potential, in which it is scaled by $k_B T$ times the number of effective persistence lengths represented by each spring.

Table 1
Summary of dimensionless parameters

Parameter	Definition	Physical interpretation
$\hat{z}_{tot}$	$\dfrac{z_{tot}}{L}$	Total z-displacement as fraction of contour length
$\hat{r}$	$\dfrac{r}{\ell}$	Radial single spring displacement as fraction of fully extended length
$\hat{f}$	$\dfrac{fA_{true}}{k_BT}$	Externally applied force in units of k_BT divided by true persistence length
α	$\dfrac{L}{A_{true}}$	Number of true persistence lengths in polymer's contour length
λ	$\dfrac{A_{eff}}{A_{true}}$	Effective persistence length in units of the true persistence length
ν	$\dfrac{\ell}{A_{true}}$	Number of true persistence lengths represented by each spring
$\hat{U}_{eff}(\hat{r})$	$\dfrac{U_{eff}(r)}{k_BT}\dfrac{\lambda}{\nu}$	Potential energy of a spring in units of k_BT times the number of effective persistence lengths represented by each spring

3.4. Force–extension results

The F–E behavior is now calculated using a general result based on Eqs. (3), (4), and (17):

$$\langle z_{tot} \rangle = k_B T \frac{\partial}{\partial f} \ln \mathcal{Z} \tag{23}$$

For bead-spring chains in particular, for which $\mathcal{Z} \to \mathcal{Z}_w$, using Eq. (19) and non-dimensionalizing with Eq. (21) shows that

$$\langle \hat{z}_{tot} \rangle_m = \frac{1}{\nu} \frac{\partial}{\partial \hat{f}} \ln \mathcal{Z}_s \tag{24}$$

where the m-subscript on the mean fractional extension is used to signify that it is for the bead-spring model. The angular integration for the single spring partition function can be performed, resulting in the following formula for the mean fractional extension:

$$\langle \hat{z}_{tot} \rangle_m = \frac{1}{\nu} \left\{ \frac{-1}{\hat{f}} + \frac{\partial}{\partial \hat{f}} \ln \left(\int_0^1 d\hat{r}\, \hat{r}\, \sinh[\nu \hat{f} \hat{r}] \right. \right.$$
$$\left. \left. \times \exp\left[\frac{-\nu}{\lambda} \hat{U}_{eff}(\hat{r}) \right] \right) \right\} \tag{25}$$

This shows explicitly that the F–E behavior of the model depends parametrically only on ν and λ, but not explicitly on the number of springs, N_s. This means that a polymer with $\alpha = 400$ represented by 40 springs has an *identical* F–E behavior as a polymer with $\alpha = 10$ represented by 1 spring because both have $\nu = 10$.

At this point it is useful to apply these definitions to the Marko and Siggia interpolation formula. It should be noted that within the context of this paper the differences between the interpolation formula and the exact numerical solution for the WLC are unimportant. Thus the polymer modelled by our so-called WLC model is not quantitatively the "true" WLC, but is a hypothetical polymer for which the Marko and Siggia formula is exact. For this polymer, the F–E behavior

is given by [10]

$$\hat{f} = \langle \hat{z}_{tot} \rangle_p - \frac{1}{4} + \frac{1}{4(1 - \langle \hat{z}_{tot} \rangle_p)^2} \tag{26}$$

where the p-subscript on the mean fractional extension signifies that it is the exact value for the polymer (to separate it from the behavior of the bead-spring model). It has been conventional for this behavior to directly motivate the following choice for the spring force-law:

$$f_{spring}(r) = \left(\frac{k_B T}{A_{eff}} \right) \left\{ \left(\frac{r}{\ell} \right) - \frac{1}{4} + \frac{1}{4(1 - r/\ell)^2} \right\} \tag{27}$$

It should be emphasized that this *assumption* has replaced the mean fractional z-projection of the polymer with the fractional radial extension of the spring. The true persistence length appearing in the polymer behavior has also been replaced by the effective persistence length in the spring force-law to use as a "correction-factor". Integrating the spring force-law gives the effective spring potential

$$U_{eff}(r) = k_B T \left(\frac{\ell}{A_{eff}} \right) \left\{ \frac{1}{2} \left(\frac{r}{\ell} \right)^2 - \frac{1}{4} \left(\frac{r}{\ell} \right) + \frac{1}{4(1 - r/\ell)} \right\} \tag{28}$$

which results in a dimensionless energy of

$$\hat{U}_{eff}(\hat{r}) = \frac{\hat{r}^2}{2} - \frac{\hat{r}}{4} + \frac{1}{4(1 - \hat{r})} \tag{29}$$

Specific examples of F–E behavior, calculated using both Eq. (25) and BD, can be seen in Fig. 3 as the level of coarse-graining, ν, is changed. The spring potential used is the Marko and Siggia interpolation formula (Eq. (29)), and for all examples in the figure the effective persistence length equals the true persistence length ($\lambda = 1$). Most of the Brownian dynamics simulations were performed using a single spring for simplicity. However, we calculate one of the points also using 20 springs to explicitly show dependence only on the level of coarse-graining, ν.

The fact that the F–E curve for a bead-spring model changes as more springs are added for a fixed contour length
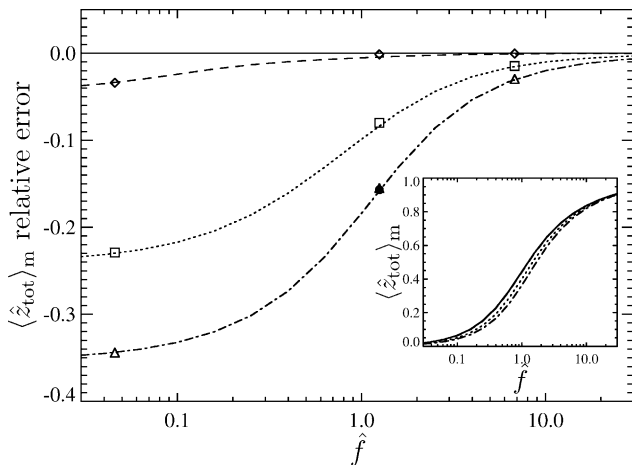
Fig. 3. Calculation of the relative error of the mean fractional extension, $(\langle \hat{z}_{tot} \rangle_m - \langle \hat{z}_{tot} \rangle_p)/\langle \hat{z}_{tot} \rangle_p$, for a bead-spring model as the level of coarse-graining changes. The Marko and Siggia potential was used with $\lambda = 1$. The curves correspond to $\nu = 400$ (dashed), $\nu = 20$ (dotted), and $\nu = 10$ (dash-dot). The symbols represent Brownian dynamics simulations. The single spring simulations correspond to $\nu = 400$ ($\diamond$), $\nu = 20$ ($\square$), and $\nu = 10$ ($\triangle$). The twenty-spring simulation corresponds to $\nu = 10$ ($\bullet$). Inset: The mean fractional extension of the models compared with the "true polymer" (solid line, Eq. (26)).

has been seen before [18]. However, the conventional explanation for this discrepancy is that the introduction of more springs directly introduces extra flexibility, which pulls in the end of chain resulting in a shorter extension for the same force. From Eq. (25) we see that this cannot be fully correct because the absolute number of springs never appears, only the level of discretization of each spring. *Thus the force–extension curve of a bead-spring chain under any conditions can be understood by only considering the behavior of a single spring, and how its force–extension behavior changes as the number of persistence lengths it represents changes.*

3.5. Phase space visualization

To get a better physical understanding of why the F–E behavior deviates from the polymer, let us examine the probability density function over the configuration space. In general for a bead-spring chain the phase space has too many dimensions to visualize easily. However as we just saw the F–E behavior can be understood by looking at a single spring, which has a phase space of only three dimensions.

Recall that the probability density is proportional to

$$\exp \left[\frac{-\mathcal{H}_{eff}}{k_B T} \right] \tag{30}$$

so that only configurations near the minimum of the effective Hamiltonian contribute significantly to the average. The configurations that contribute must have a $\mathcal{H}_{eff}$ less than $k_B T$ above the minimum:

$$\mathcal{H}_{eff} = (\mathcal{H}_{eff})_{min} + O(k_B T) \tag{31}$$

For the case of a single spring as considered here the effective Hamiltonian is

$$\mathcal{H}_{eff} = U_{eff}(r) - fz = k_B T \nu \left(\frac{\hat{U}_{eff}(\hat{r})}{\lambda} - \hat{f}\hat{z} \right) \tag{32}$$

and therefore the important configurations are determined by

$$\hat{\mathcal{H}}_{eff} \equiv \left(\frac{\hat{U}_{eff}(\hat{r})}{\lambda} - \hat{f}\hat{z} \right) = \left(\frac{\hat{U}_{eff}(\hat{r})}{\lambda} - \hat{f}\hat{z} \right)_{min} + O\left(\frac{1}{\nu} \right) \tag{33}$$

where we have defined a dimensionless effective Hamiltonian, $\hat{\mathcal{H}}_{eff}$. From Eq. (33) we see that $1/\nu$ plays a similar role in the F–E behavior as temperature usually does in statistical mechanics, determining the magnitude of fluctuations in phase space about the minimum. A detailed and quantitative description of fluctuations will be performed later in Section 3.7. Here we will discuss how the portion of phase space the system samples (fluctuates into) with significant probability determines the mean extension. In the limit $\nu \to \infty$, the system is "frozen-out" into the state of minimum $\hat{\mathcal{H}}_{eff}$. Note that as $\nu \to \infty$, the polymer becomes infinitely long. By calculating the *fractional* extension, we are scaling all lengths by the contour length. Thus even though the fluctuations may not be getting small if a different length scale were used (such as the radius of gyration), the fluctuations of the end-to-end distance do go to zero compared to the contour length. Alternatively in the limit $\nu \to 0$, the system is equally likely to be in any state, and thus the mean fractional extension of the bead-spring chain, $\langle \hat{z}_{tot} \rangle_m$, approaches zero.

In order to understand the behavior at intermediate ν, Fig. 4 shows a contour plot of $\hat{\mathcal{H}}_{eff}$ for the four cases $\hat{f} = 0.444$, $\hat{f} = 5$, $\lambda = 1$, and $\lambda = 1.5$, and the Marko and Siggia spring potential (Eq. (29)). The contour lines correspond to lines of constant $\hat{\mathcal{H}}_{eff}$ within the $\hat{x}$–$\hat{z}$ plane. Note that because all directions perpendicular to $\hat{z}$ are equivalent, rotating the contour lines about the $\hat{z}$ axis produces surfaces in the three-dimensional phase space with constant $\hat{\mathcal{H}}_{eff}$. While $\hat{\mathcal{H}}_{eff}$, and therefore the contour plots, are independent of ν, they can be used to understand the behavior at different values of ν because of Eq. (33). The value of ν governs the size of the fluctuations around the minimum, and thus the number of contour lines above the minimum the system samples with significant probability. We also see that each of the $\hat{\mathcal{H}}_{eff}$ contours is not symmetric about the minimum of $\hat{\mathcal{H}}_{eff}$, causing the mean extension of the bead-spring chain, $\langle \hat{z}_{tot} \rangle_m$, to deviate from the point of minimum $\hat{\mathcal{H}}_{eff}$. For $\lambda = 1$ the minimum of $\hat{\mathcal{H}}_{eff}$ corresponds to the mean extension of the true polymer, $\langle \hat{z}_{tot} \rangle_p$. This is because of the way of choosing the spring potential from the true polymer behavior as illustrated with Eqs. (26)–(29). As λ is increased, the position of the minimum moves to larger $\hat{z}$ while the depth of the minimum increases. The minimum also moves to larger $\hat{z}$ and deepens when the force is increased. These plots explain why as $\nu \to \infty$ the bead-spring chain behavior only approaches the true polymer behavior if $\lambda = 1$, why as $\nu \to 0$ the mean frac-
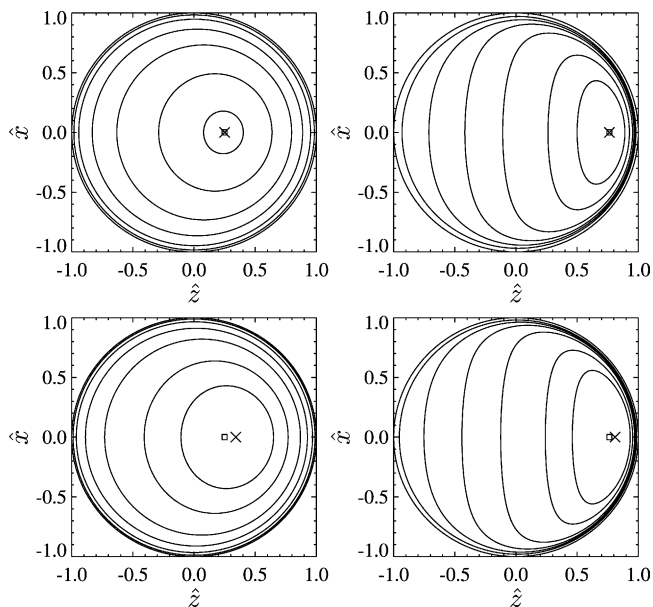
Fig. 4. Visualization of phase space using contours of constant $\hat{\mathcal{H}}_{\text{eff}}$ for a single spring with the Marko and Siggia potential. The square ($\square$) represents the position of the "true polymer" mean fractional extension, $\langle \hat{z}_{\text{tot}} \rangle_{\text{p}}$. The cross ($\times$) represents the position of minimum $\hat{\mathcal{H}}_{\text{eff}}$. Upper left: $\hat{f} = 0.444$, $\lambda = 1$; lower left: $\hat{f} = 0.444$, $\lambda = 1.5$; upper right: $\hat{f} = 5$, $\lambda = 1$; lower right: $\hat{f} = 5$, $\lambda = 1.5$.

tional extension approaches zero, and why for intermediate ν there may exist a value of λ for which the mean fractional extension matches the true polymer.

3.6. Correcting the force–extension behavior

Now that we understand better the reasons why the F–E curve deviates from the true polymer F–E curve, we would like to change the model to get closer agreement. A very simple method that has been used by previous investigators [18] is to use a different persistence length in the spring force-law (A_{eff}) from the true persistence length of the polymer (A_{true}), i.e. $\lambda \neq 1$. In particular, if λ is increased, the extension of the chain also increases, back to the extension of the true polymer. The conventional explanation for this is that the free hinges in the bead-spring chain have introduced extra flexibility. To counter-act the flexibility introduced by the hinges, the stiffness of the springs must be increased by increasing the effective persistence length. Let us now analyze the effect of increasing λ within the framework presented above. Looking at Eq. (25) shows that increasing λ acts to decrease the spring potential energy. Because the spring gets weaker (less stiff), it is not surprising that the extension gets larger. It should be noted that for infinitely long polymers increasing the persistence length causes a decrease in the restoring force.

Though it is true that by increasing λ from one the extension increases towards the true extension of the polymer, it does so non-uniformly. This means that there exists no value

of λ such that the F–E curve exactly matches the true curve. It is unclear what value of λ to choose to give the "best fit" between the model curve and the true curve. We will present here an analysis of possible choices and place bounds on the range of choices. The first criterion that might come to mind is some type of integrated sum of squared error. However, that quantity becomes very cumbersome to manipulate analytically and it is unclear that it is any better of a criterion than another. The criteria that we will consider looks at matching exactly one section of the F–E curve. The three sections are at zero applied force, at infinite applied force, and at the applied force for which the true polymer has a mean fractional extension of 0.5. Before calculations can be made of the "best-fit" λ in each region, the exact meaning of matching the true polymer behavior must be specified. The half-extension criterion is straight-forward: we will require that the model and polymer curves are equal at the point where the polymer is at half extension. The other two criteria are more subtle because the model and polymer become equal at zero and infinite force for all values of λ. For the low-force criterion we will require that the slopes of the F–E curves be equal at zero force. It should be noted that this is equivalent to requiring that the relative error of the model goes to zero at zero force. Again, a similar criterion cannot be used at infinite force because the slope (or relative error) will always be zero at infinity independent of λ. Thus our infinite force criteria will be that the relative error of the slope of the F–E curve at infinite force will equal zero. Physically, this means that the fractional extension versus force curves approach one at infinite force in the same manner. Fig. 5 shows a plot of the "best-fit" λ versus $1/\nu$ for each of the three criteria for the WLC force-law.
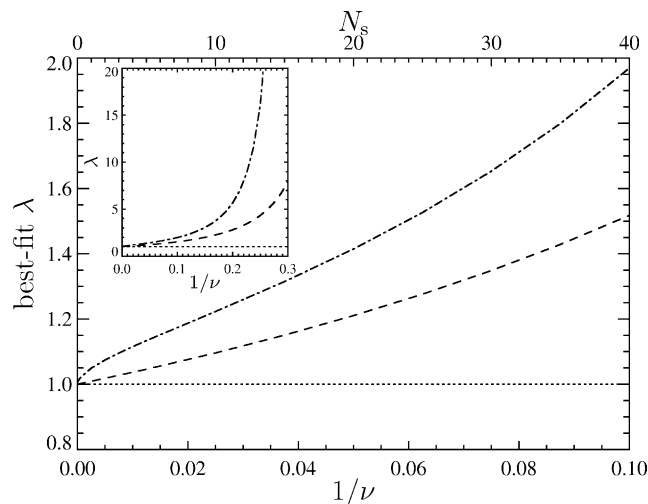

Fig. 5. Calculation of λ for the three different criteria at different levels of coarse-graining for the Marko and Siggia potential. The criteria shown are low-force (dash-dot), half-extension (dashed), and high-force (dotted). Upper axis: the level of coarse-graining in terms of the number of springs, N_{s}, for a polymer with $\alpha = 400$ (approximately λ-phage DNA stained with YOYO at 4 bp:1 dye molecule). Inset: expanded view showing the divergence of the criteria.

It is important to mention that both the low-force and half-extension curves diverge for a finite $1/\nu$. This means that there exists a ν small enough such that the low-force or half-extension region cannot be matched simply by adjusting λ. The position of these divergences can be calculated *exactly* in a simple manner as will be shown in Section 3.8. For the WLC the low-force curve diverges at $\nu^* = 10/3$ while the half-extension curve diverges at $\nu^* = 2.4827$. However the high-force curve is always $\lambda = 1$ for finite $1/\nu$.

To illustrate the difference between the three choices of λ, let us look at a specific example. Fig. 6 shows the relative error in the mean fractional extension versus force for the WLC force-law, three different values of λ, and $\nu = 20$. The three values of λ correspond to the three criteria shown in Fig. 5. By comparing the relative error curves, we can see the entire range of effects λ has on the F–E behavior. The criteria at low and high force form a bound on the choices for a "best-fit" λ as seen in Fig. 6, even if none of the criteria presented here is believed best.

As a further example we show the parameters that would be chosen to model λ-phage DNA at different levels of coarse-graining, as well as some properties of the models. These parameters could be used in a Brownian dynamics simulation to capture the non-equilibrium properties of λ-phage DNA. Tables 2–4 show what effective persistence length to choose for the model for the different "best-fit" criteria and for different staining ratios of dye. The parameters were calculated by repeated application of Fig. 5. The result-
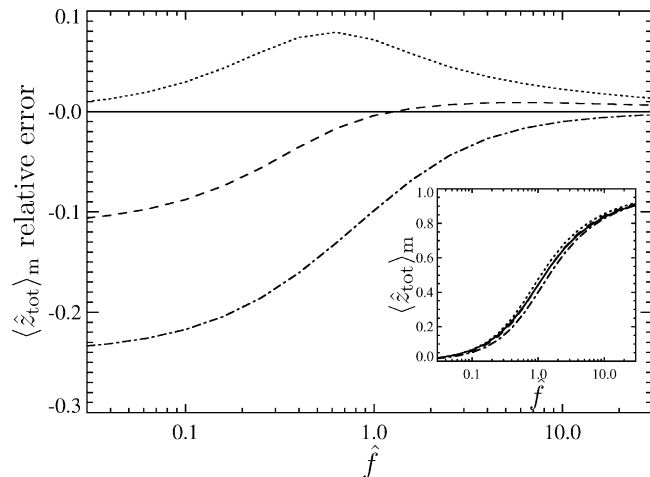

Fig. 6. Calculation of the relative error of the mean fractional extension, $(\langle \hat{z}_{\mathrm{tot}}\rangle_{\mathrm{m}} - \langle \hat{z}_{\mathrm{tot}}\rangle_{\mathrm{p}})/\langle \hat{z}_{\mathrm{tot}}\rangle_{\mathrm{p}}$, for a bead-spring model for different best fit criteria. The Marko and Siggia potential was used with $\nu = 20$. The curves correspond to $\lambda = 1.41$ (low-force, dotted), $\lambda = 1.21$ (half-extension, dashed), and $\lambda = 1$ (high-force, dash-dot). Inset: the mean fractional extension of the models compared with the "true polymer" (solid line, Eq. (26)).

ing properties of the model were calculated from formulae in Section 4. The contour length and persistence length for unstained λ-phage DNA were taken from Bustamante et al. [29]. We used that the contour length is increased by 4 Å per bis-intercalated YOYO dye molecule [30], and we assumed

Table 2
Table of properties for models of unstained λ-phage DNA

N_s	ν	Region	λ	A_{eff} (μm)	R_g (μm)	$\eta_{0,\mathrm{p}}/(n_{\mathrm{p}}(N\zeta))$ (μm^2)	$b_2/(n_{\mathrm{p}}(N\zeta)^2/k_BT)$ (μm^4)	$\tau_0/((N\zeta)/k_BT)$ (μm^2)
10	30.8	Low	1.28	0.068	0.56	0.052	−0.0011	0.021
		Mid	1.13	0.060	0.53	0.047	−0.00091	0.019
		High	1.0	0.053	0.50	0.042	−0.00074	0.017
20	15.4	Low	1.55	0.082	0.55	0.050	−0.0010	0.020
		Mid	1.29	0.068	0.51	0.044	−0.00077	0.018
		High	1.0	0.053	0.47	0.036	−0.00052	0.014
40	7.7	Low	2.52	0.133	0.54	0.049	−0.00096	0.019
		Mid	1.78	0.094	0.50	0.041	−0.00068	0.016
		High	1.0	0.053	0.42	0.029	−0.00034	0.012

Unstained λ-phage DNA has the following properties: $L = 16.3$ μm, $A_{\mathrm{true}} = 0.053$ μm, and $\alpha = 307.5$. Models with 10, 20, and 40 springs are compared using three best-fit λ criteria.

Table 3
Table of properties for models of λ-phage DNA stained with YOYO at 8 bp:1 dye molecule

N_s	ν	Region	λ	A_{eff} (μm)	R_g (μm)	$\eta_{0,\mathrm{p}}/(n_{\mathrm{p}}(N\zeta))$ (μm^2)	$b_2/(n_{\mathrm{p}}(N\zeta)^2/k_BT)$ (μm^4)	$\tau_0/((N\zeta)/k_BT)$ (μm^2)
10	35.3	Low	1.25	0.066	0.60	0.060	−0.0015	0.025
		Mid	1.11	0.059	0.57	0.054	−0.0012	0.022
		High	1.0	0.053	0.55	0.050	−0.0010	0.020
20	17.6	Low	1.47	0.078	0.59	0.058	−0.0013	0.023
		Mid	1.24	0.066	0.55	0.051	−0.0010	0.020
		High	1.0	0.053	0.51	0.043	−0.00073	0.017
40	8.8	Low	2.18	0.116	0.58	0.056	−0.0013	0.022
		Mid	1.62	0.086	0.54	0.048	−0.00091	0.019
		High	1.0	0.053	0.46	0.035	−0.00049	0.014

Models with 10, 20, and 40 springs are compared using three best-fit λ criteria. 8 bp:1 dye λ-phage DNA has the following properties: $L = 18.7$ μm, $A_{\mathrm{true}} = 0.053$ μm, and $\alpha = 352.8$.

Table 4
Table of properties for models of λ-phage DNA stained with YOYO at 4 bp:1 dye molecule

N_s	ν	Region	λ	A_{eff} (µm)	R_g (µm)	$\eta_{0,p}/(n_p(N\zeta))$ (µm²)	$b_2/(n_p(N\zeta)^2/k_BT)$ (µm⁴)	$\tau_0/((N\zeta)/k_BT)$ (µm²)
10	39.8	Low	1.22	0.065	0.64	0.068	−0.0019	0.028
		Mid	1.10	0.058	0.61	0.062	−0.0016	0.025
		High	1.0	0.053	0.58	0.057	−0.0013	0.023
20	19.9	Low	1.42	0.075	0.62	0.065	−0.0017	0.026
		Mid	1.21	0.064	0.59	0.058	−0.00013	0.023
		High	1.0	0.053	0.54	0.049	−0.00097	0.020
40	9.95	Low	1.98	0.105	0.62	0.064	−0.0016	0.025
		Mid	1.52	0.081	0.57	0.054	−0.0012	0.022
		High	1.0	0.053	0.50	0.041	−0.00067	0.016

Models with 10, 20, and 40 springs are compared using three best-fit λ criteria. 4 bp:1 dye λ-phage DNA has the following properties: $L = 21.1$ µm, $A_{\text{true}} = 0.053$ µm, and $\alpha = 398.1$.

that the persistence length of the stained molecule is the same as the unstained value.

In these tables we see examples of the expected general trends. As the polymer is more finely discretized, the number of persistence lengths represented by each spring, ν, decreases. This causes a larger spread in the possible choices for the effective persistence length, and thus a larger spread in properties. We see the general trend that the magnitude of the properties decreases as ν decreases. Note that for the low-force criterion, R_g and $\eta_{0,p}$ are exactly the "Rouse result". The "Rouse Result" is the value of the Rouse model if the spring constant is taken to be the zero-extension slope of the *spring* force-law. The "Rouse result" will be discussed in more detail in Section 4. The only difference from the "true polymer" is that the mass and drag are localized at the beads instead of along a continuous contour. This is true until ν reaches the point of divergence of the low-force criterion. However, b_2 and τ_0 are only approximately the "Rouse result" as discussed in Section 4. The properties for the other best-fit criteria have even smaller magnitude than the low-force criterion. This decrease is due to an error in the zero-force slope of the force–extension curve, and thus a smaller coil size.

3.7. Fluctuations

In addition to discussing the F–E behavior of the model, it is important to discuss the fluctuations around the mean extension. We have already seen the use of fluctuations thus far. In Section 3.5 we saw how examining fluctuations can help us better understand the *mean* extension. The fluctuations in the F–E behavior are also important in trying to extend our understanding from the F–E behavior of the bead-spring chains to the behavior in a flow field. For a bead-spring chain in a flow field, the fluctuations of the chain determine how much of the flow field the chain can sample. In turn this determines the total force applied to the chain by the flow. This is particularly important in shear flow, in which the fluctuation of the chain in the shear gradient direction plays a central role [8,31].

It is shown in Appendix A that the fluctuations can be calculated as

$$(\delta\hat{z})^2 = \langle(\hat{z}_{\text{tot}} - \langle\hat{z}_{\text{tot}}\rangle_m)^2\rangle_m = \frac{1}{N_s\,\nu}\frac{\partial}{\partial\hat{f}}\langle\hat{z}_{\text{tot}}\rangle_m$$

$$= \frac{1}{\alpha}\frac{\partial}{\partial\hat{f}}\langle\hat{z}_{\text{tot}}\rangle_m \tag{34}$$

$$(\delta\hat{x})^2 = \langle(\hat{x}_{\text{tot}})^2\rangle_m = \langle(\hat{y}_{\text{tot}})^2\rangle_m = \frac{1}{N_s\,\nu\,\hat{f}}\langle\hat{z}_{\text{tot}}\rangle_m$$

$$= \frac{1}{\alpha\,\hat{f}}\langle\hat{z}_{\text{tot}}\rangle_m \tag{35}$$

where we have defined the root-mean-squared fluctuations as $\delta\hat{z}$ and $\delta\hat{x}$. One important thing to notice about the fluctuations is that once the F–E behavior is known ($\langle\hat{z}_{\text{tot}}\rangle_m$ versus $\hat{f}$), the fluctuations can be calculated directly without performing any further integrations. In fact, both types of fluctuations can be calculated by finding the slope of a line on the F–E curve, as seen in Fig. 7. From the figure we see that the longitudinal fluctuations are proportional to the slope of the curve, while the lateral fluctuations are proportional to the slope of the line connecting the point of the F–E curve to the origin. Because the F–E curve is concave, *the lateral fluctuations are always greater than or equal to the longitudinal fluctuations.*

Another important aspect of Eqs. (34) and (35) is that the fluctuations depend explicitly on the number of springs in the chain, unlike the F–E curve which just depends on the level of coarse-graining for each spring. In fact we see the expected scaling of the root-mean-squared fluctuations as $\alpha^{-1/2}$. Since the persistence length is the length-scale over which the polymer backbone loses correlation, the fluctuation of the polymer length should scale like a sum of "independent" random variables. The number of these "independent" random variables is precisely the number of persistence lengths in the polymer contour, α. We show in Figs. 8 and 9 plots of the root-mean-squared fluctuations for the same cases for which we showed the F–E behavior in Fig. 3. We have scaled the fluctuations by $\alpha^{1/2}$ to collapse the fluctuations of different length chains onto the same curve. The fluctuations after this scaling only
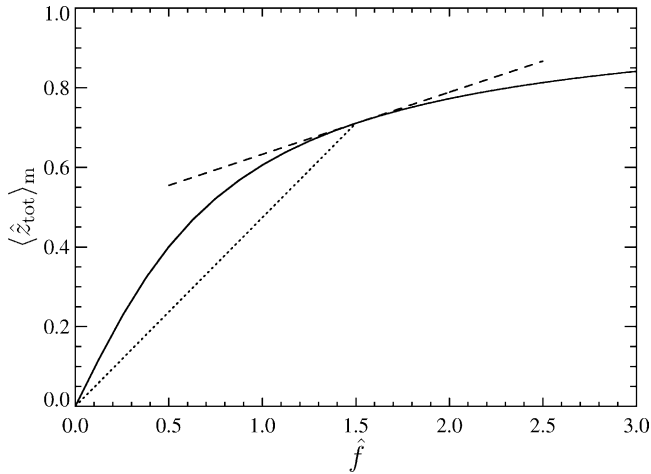
Fig. 7. Graphical illustration of longitudinal and transverse fluctuations. For a given force $\hat{f}$, the longitudinal fluctuations are proportional to the slope of the tangent curve (dashed). The transverse fluctuations are proportional to the slope of the chord (dotted) connecting the origin to the point on the force–extension curve.

depend on the number of persistence lengths represented by each spring, ν, and the ratio of the effective persistence length to the true persistence length, λ.

Note that it is easy to calculate exactly the high-force scalings for the fluctuations using Eqs. (34) and (35) and our knowledge of the high-force scaling for $\langle \hat{z}_{tot} \rangle_m$. It is easy to show that for bead-spring chains using the Marko and Siggia potential (Eq. (29)) the high-force scaling is

$$\langle \hat{z}_{tot} \rangle_m \overset{\hat{f} \to \infty}{\sim} 1 - \frac{1}{2\lambda^{1/2} \hat{f}^{1/2}} + O\left(\frac{1}{\hat{f}}\right) \tag{36}$$
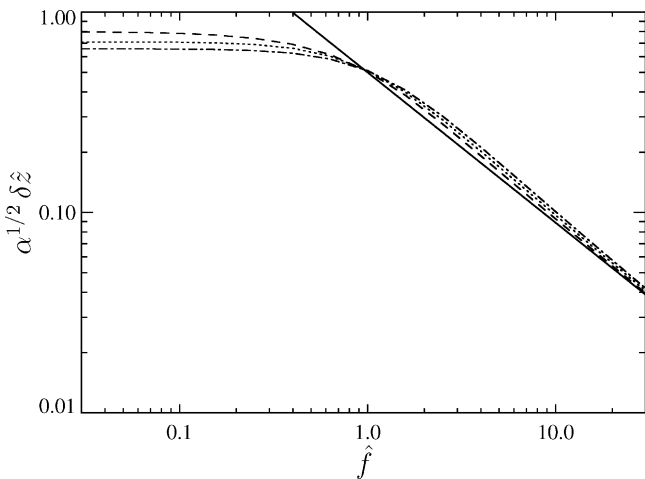
Fig. 8. Calculation of the longitudinal root-mean-squared fluctuations at different levels of coarse-graining. The Marko and Siggia potential was used with $\lambda = 1$. The curves correspond to $\nu = 400$ (dashed), $\nu = 20$ (dotted), and $\nu = 10$ (dash-dot). The solid line corresponds to the high-force asymptotic behavior, $1/(2\hat{f}^{3/4})$.
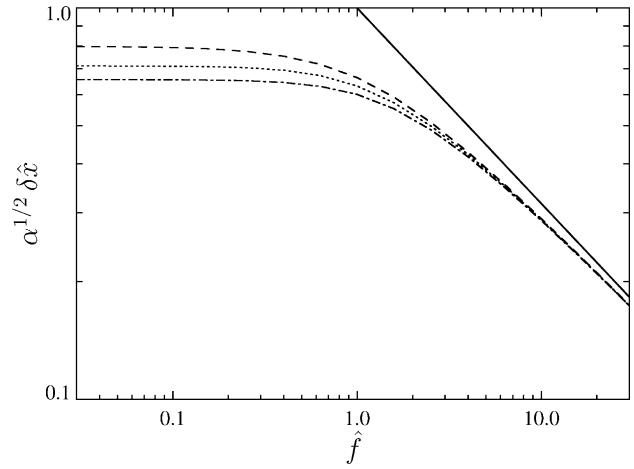

Fig. 9. Calculation of the transverse root-mean-squared fluctuations at different levels of coarse-graining. The Marko and Siggia potential was used with $\lambda = 1$. The curves correspond to $\nu = 400$ (dashed), $\nu = 20$ (dotted), and $\nu = 10$ (dash-dot). The solid line corresponds to the high-force asymptotic behavior, $1/(\hat{f}^{1/2})$.

Using this result, we can show that

$$\alpha^{1/2} \delta \hat{z} \overset{\hat{f} \to \infty}{\sim} \frac{1}{2\lambda^{1/4} \hat{f}^{3/4}} + O\left(\frac{1}{\hat{f}^{5/4}}\right) \tag{37}$$

$$\alpha^{1/2} \delta \hat{x} \overset{\hat{f} \to \infty}{\sim} \frac{1}{\hat{f}^{1/2}} + O\left(\frac{1}{\hat{f}}\right) \tag{38}$$

Of particular interest are the fluctuations at "equilibrium" (zero applied force) because it relates to the size of the polymer coil. In the context of the F–E behavior, that is equivalent to calculating the slope of the F–E curve at zero force, as can be seen by taking the limit $\hat{f} \to 0$ in Eqs. (34) or (35). By taking that limit, and rewriting the average as the average of the radial coordinate of a single spring, it can be shown that

$$\lim_{\hat{f} \to 0} \left(\frac{\partial}{\partial \hat{f}} \langle \hat{z}_{tot} \rangle_m \right) = \frac{\nu}{3} \frac{\int_0^1 d\hat{r} \, \hat{r}^4 \, \exp[-(\nu/\lambda) \, \hat{U}_{eff}(\hat{r})]}{\int_0^1 d\hat{r} \, \hat{r}^2 \, \exp[-(\nu/\lambda) \, \hat{U}_{eff}(\hat{r})]} \tag{39}$$

This expression was used previously in Section 3.6 to calculate the "best-fit" λ at zero force as seen in Fig. 5, and it will be used extensively to understand rheological properties in Section 4.

We also note here that Ladoux and Doyle [31] derived an expression similar to Eq. (35) based on scaling arguments and a single spring. Based on the scaling argument, they developed a model which compared favorably to experimental data and lends support to the results presented here.

3.8. Limiting behavior (asymptotic expansions)

We have seen thus far that the F–E behavior of bead-spring chains can be written analytically as integral formulae for arbitrary spring force-law. This has allowed for the determination of the important dimensionless groups that determine the behavior, as well as provide for rapid and accurate calculation

through numerical integration. However, another important advantage to having analytical formulae is that expansions can be performed. Those expansions can be used to illustrate limiting and universal behavior as well as obtain approximate algebraic formulae that illustrate what aspects of the force-law are needed to estimate the exact behavior without performing numerical integration.

We have already seen numerically in Fig. 3 that the F–E behavior of the model only matches the "true" polymer behavior if each spring represents a large number of persistence lengths. Thus it seems natural to find asymptotic expansions of the integrals in the limit $\nu \to +\infty$. We start by expanding directly the force–extension curve (Eq. (25)). The asymptotic expansion is a straightforward application of Laplace's Method [32]. The calculation is made significantly easier by noting that the hyperbolic sine can be replaced by only the growing exponential, because it only results in subdominant corrections. Up to first order, the expansion is given by

$$\langle \hat{z}_{\text{tot}} \rangle_{\text{m}} \overset{\nu \to \infty}{\sim} c + \frac{1}{\nu} \left[\frac{-1}{\hat{f}} + \frac{1}{c} \left(\frac{\partial c}{\partial \hat{f}} \right) + \frac{(\partial^2 c / \partial \hat{f}^2)}{2(\partial c / \partial \hat{f})} \right]$$
$$+ \mathrm{O}\left(\frac{1}{\nu^2} \right) \quad (40)$$

where

$$c \equiv \langle \hat{z}_{\text{tot}} \rangle_{\text{p}} (\lambda \hat{f}) \quad (41)$$

We thus see again that as $\nu \to \infty$ with $\lambda = 1$ the F–E behavior of the bead-spring model approaches the true polymer. However, we also have the correction terms written as a function of the *true polymer* F–E curve. *No assumption* has been made about the spring force-law other than it is determined from the "true polymer" F–E behavior as was done for the WLC model in Section 3.4. Provided the value of ν is "large enough", Eq. (40) can be used to estimate the F–E behavior of a bead-spring model without performing any numerical integrations for any value of $\hat{f}$ or λ within

$$0 < \hat{f} < \infty, \qquad 0 < \lambda < \infty \quad (42)$$

To give a sense of the applicability of the expansion in Eq. (40) to smaller ν, we show in Fig. 10 a comparison of the exact force-extension result for the Marko and Siggia potential with $\lambda = 1$ and the asymptotic expansion for forces $\hat{f} = 0.1$ and $\hat{f} = 1.25$. We see that the expansion is applicable to smaller ν when $\hat{f}$ is larger. The zero-one Padé approximant $P_1^0(1/\nu)$ is seen to improve the small ν behavior.

Care must be taken if Eq. (40) is expanded for large or small $\hat{f}$ because of the order in which limits are taken. If the F–E curve is expanded to $\mathrm{O}(\nu^{-a})$, then the asymptotic expansion $\hat{f} \to \infty$ can only be obtained to $\mathrm{O}(\hat{f}^{-a})$. At low force, the quantity of greatest interest is the slope of the F–E curve at zero force, given by Eq. (39). In general, expanding Eq. (39) directly for $\nu \to \infty$ gives a different result from expanding Eq. (40) for small $\hat{f}$. The expansions are the same
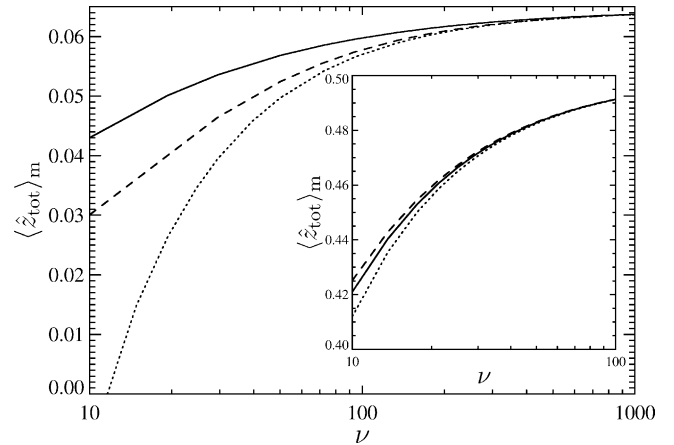

Fig. 10. Comparison of the fractional extension with its high ν asymptotic expansion for the Marko and Siggia potential with $\lambda = 1$ and $\hat{f} = 0.1$. The curves correspond to the exact result (solid line), the expansion including $\mathrm{O}(1/\nu)$ (dotted), and the zero-one Padé $P_1^0(1/\nu)$ (dashed). Inset: the analogous comparison for $\hat{f} = 1.25$.

if and only if the spring force-law is an odd function of its argument (the potential is an even function).

Even for the case of an odd spring force-law, it is more computationally convenient to obtain the expansion of the slope of the F–E curve at zero force directly by expanding Eq. (39). Application of Laplace's Method requires the expansion of the spring force-law, of the following form:

$$\hat{U}_{\text{eff}}(\hat{r}) = \phi_0 + \phi_2 \hat{r}^2 + \hat{r}^3 \sum_{i=0}^{\infty} h_i \hat{r}^i \quad (43)$$

Note that there is no linear term because we require this potential to look Hookean near $\hat{r} = 0$ and that the value of the constant term, ϕ_0, does not affect the final answer. Also note that $\phi_2 > 0$.

Proceeding with Laplace's Method, the complete asymptotic series can be calculated to be the following:

$$\lim_{\hat{f} \to 0} \left(\frac{\partial}{\partial \hat{f}} \langle \hat{z}_{\text{tot}} \rangle_{\text{m}} \right) \overset{\nu \to +\infty}{\sim} \left(\frac{\lambda}{2\phi_2} \right) \times \sum_{i=0}^{\infty} d_i \left(\frac{\lambda}{\nu \phi_2} \right)^{i/2} \quad (44)$$

The coefficients of the series can be calculated from a collection of recursion relations that include the coefficients of the Taylor series of the spring potential. The recursion relations are given here for completeness:

$$d_0 = \frac{F_0^{(4)}}{F_0^{(2)}} = 1,$$

$$d_i = \frac{1}{F_0^{(2)}} \left(F_i^{(4)} - \sum_{m=0}^{i-1} d_m F_{i-m}^{(2)} \right)$$
$$= F_i^{(4)} - \sum_{m=0}^{i-1} d_m F_{i-m}^{(2)}, \quad i \geq 1 \quad (45)$$

$$F_i^{(n)} = \left[\sum_{j=0}^{i} {}_{(j)}G_{(i-j)} \left(\frac{-1}{\phi_2} \right)^j \left(\frac{\Gamma(j + i/2 + (n+1)/2)}{j!\,\Gamma((n+1)/2)} \right) \right]$$

$$\tag{46}$$

$${}_{(m)}G_{(n)} = \sum_{i=0}^{n} {}_{(m-1)}G_{(i)}h_{(n-i)},$$

$$n = 0, 1, 2, \ldots, \quad m = 1, 2, 3, \ldots,$$

$${}_{(0)}G_{(0)} = 1, \quad {}_{(0)}G_{(1,2,\ldots)} = 0 \tag{47}$$

We have also examined the ability to use this expansion at smaller ν, as shown in Fig. 11 for the Marko and Siggia potential with $\lambda = 1$. It should be noted that the zero-one Padé $P_1^0(1/\nu^{1/2})$ performs worse than the first two terms of the expansion in Eq. (44). However, the two-point zero-two Padé $P_2^0(1/\nu^{1/2})$ that includes the behavior at small ν does perform better. This low ν behavior will now be discussed.

In addition to examining the bead-spring chains in the limit $\nu \to \infty$, it is interesting to examine the F–E behavior in the limit $\nu \to 0$. In this limit the F–E behavior can approach a curve *independent* of the functional form of $\hat{U}_{\text{eff}}(\hat{r})$. Physically one can think of this limit as taking a polymer with fixed contour length, and infinitely discretizing the model. Therefore each spring is becoming very small. However, it should also be noted that each spring is getting weaker, as seen in Eq. (32). It has been postulated previously that as the chain is infinitely discretized, the F–E behavior would approach that of the freely jointed chain [18]. Using the formalism presented thus far, we can examine explicitly this limit and test the postulated behavior. To understand the F–E behavior in this limit, we simply need to expand Eq. (25) for $\nu \to 0$.

It should first be noted that expanding the prescribed integral is an example of an integral that can only be expanded

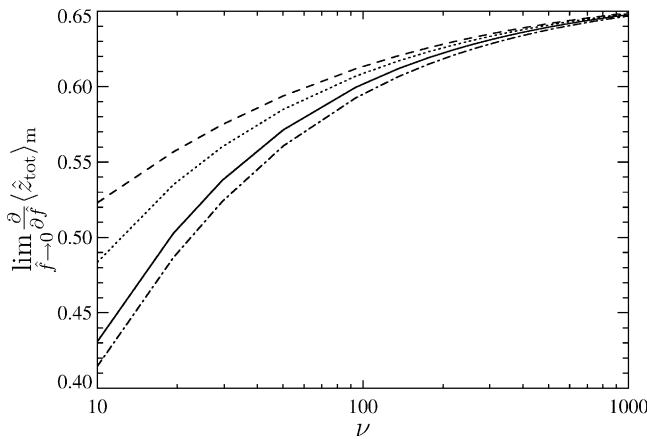Fig. 11. Comparison of the zero-force slope with its high ν asymptotic expansion for the Marko and Siggia potential with $\lambda = 1$. The curves correspond to the exact result (solid line), the expansion including $O(1/\nu^{1/2})$ (dotted), the zero-one Padé $P_1^0(1/\nu^{1/2})$ (dashed), and the two-point zero-two Padé $P_2^0(1/\nu^{1/2})$ (dash-dot).

rigorously using asymptotic matching, but the leading-order behavior is relatively easy to obtain [32]. In fact, the leading order behavior is obtained by setting

$$\exp\left[\frac{-\nu}{\lambda} \hat{U}_{\text{eff}}(\hat{r}) \right] \simeq 1 \tag{48}$$

By further expanding the hyperbolic sine, it can be easily shown that

$$\langle \hat{z}_{\text{tot}} \rangle_{\text{m}} \overset{\nu \to 0}{\sim} \frac{\nu \hat{f}}{5}, \quad \hat{f} \text{ fixed} \tag{49}$$

Note that this is consistent with Section 3.5 in which we saw that, for $\hat{f}$ fixed, the mean fractional extension approaches zero as $\nu \to 0$. We also see explicitly that the F–E behavior *does not* approach the FJC, which is given by

$$\langle \hat{z}_{\text{tot}} \rangle_{\text{m}} = \mathcal{L}(\hat{f}) \tag{50}$$

where

$$\mathcal{L}(x) = \coth(x) - \frac{1}{x} \tag{51}$$

is the Langevin function. We can also contrast the behavior in Eq. (49) with a different "experiment" in which free hinges are introduced into a true *continuous* worm-like chain while the force is held constant. If one considers ν to be the ratio of the contour length of the continuous curve between free hinges to the persistence length, then it is clear that the average extension of this discretized worm-like chain, $\langle \hat{z}_{\text{tot}} \rangle_{\text{dwlc}}$, approaches the limit

$$\langle \hat{z}_{\text{tot}} \rangle_{\text{dwlc}} \overset{\nu \to 0}{\sim} \mathcal{L}(\nu \hat{f}) \overset{\nu \to 0}{\sim} \tfrac{1}{3}(\nu \hat{f}), \quad \hat{f} \text{ fixed} \tag{52}$$

It should be noted that holding $\hat{f}$ fixed corresponds to the physical process of holding the force constant as the model is infinitely discretized. This is the appropriate limit to examine processes in which the force applied to the end of the system is independent of how the system is discretized. However, another universal result can be obtained by instead of holding $\hat{f}$ fixed, holding $\nu \hat{f}$ fixed. This corresponds to pulling harder and harder on the model as it is more finely discretized. One might expect that the length of a spring should play the role of the "Kuhn length", and thus the scale for the force. This corresponds to a dimensionless force of $\nu \hat{f}$. The expansion of the bead-spring chain model behavior with $\nu \hat{f}$ fixed is calculated by simply integrating the hyperbolic sine in Eq. (25) to obtain

$$\langle \hat{z}_{\text{tot}} \rangle_{\text{m}} \overset{\nu \to 0}{\sim} \frac{-3}{\nu \hat{f}} + \frac{1}{\mathcal{L}(\nu \hat{f})}, \quad (\nu \hat{f}) \text{ fixed} \tag{53}$$

We see that even in this limit the system *does not* approach a modified "freely jointed chain" result of

$$\langle \hat{z}_{\text{tot}} \rangle_{\text{m}} = \mathcal{L}(\nu \hat{f}) \tag{54}$$

To understand the true limiting shape (Eq. (53)) it can be shown that

$$\frac{-3}{x} + \frac{1}{\mathcal{L}(x)} \approx \mathcal{L}\left(\frac{x}{2}\right), \quad x \text{ large} \tag{55}$$

$$\frac{-3}{x} + \frac{1}{\mathcal{L}(x)} \approx \mathcal{L}\left(\frac{3x}{5}\right), \quad x \text{ small} \tag{56}$$

In addition to being used to understand the limit of infinite discretization, Eq. (53) can be used to understand the divergence of the "best-fit" λ curves in Fig. 5 and discussed in Section 3.6. Recall that previously we considered the limit in Eq. (53) to be as $\nu \to 0$ as $(\nu \hat{f})$ was held fixed, and λ was implicitly being held constant. By examining Eq. (25), we see that if $(\nu \hat{f})$ is held constant, the only remaining parameter is ν/λ. Thus the expression in Eq. (53) can be rewritten as the limit $(\nu/\lambda) \to 0$:

$$\langle \hat{z}_{\text{tot}} \rangle_{\text{m}} \overset{\lambda \to \infty}{\sim} \frac{-3}{\nu \hat{f}} + \frac{1}{\mathcal{L}(\nu \hat{f})}, \quad \text{both } \nu, \hat{f} \text{ fixed} \tag{57}$$

Now suppose that one is choosing λ such that the model matches the true polymer at an extension of $\langle \hat{z}_{\text{tot}} \rangle_{\text{p}}$, which occurs at a force denoted $\hat{f}(\langle \hat{z}_{\text{tot}} \rangle_{\text{p}})$. The value of ν for which that "best-fit" curve diverges (denoted ν^*) will be the value for which only as $\lambda \to \infty$ will the extension of the model equal that of the polymer. This condition is written as

$$\langle \hat{z}_{\text{tot}} \rangle_{\text{p}} = \frac{-3}{\nu^* \hat{f}(\langle \hat{z}_{\text{tot}} \rangle_{\text{p}})} + \frac{1}{\mathcal{L}(\nu^* \hat{f}(\langle \hat{z}_{\text{tot}} \rangle_{\text{p}}))} \tag{58}$$

This can also be used to find the divergence of the low force criteria by examining the limit as $\hat{f} \to 0$. Because of the way of choosing the force-law from the true polymer behavior, it can be shown easily that

$$\langle \hat{z}_{\text{tot}} \rangle_{\text{p}} \overset{\hat{f} \to 0}{\sim} \frac{\hat{f}}{2\phi_2} \tag{59}$$

It can also be shown that

$$\frac{-3}{\nu^* \hat{f}(\langle \hat{z}_{\text{tot}} \rangle_{\text{p}})} + \frac{1}{\mathcal{L}(\nu^* \hat{f}(\langle \hat{z}_{\text{tot}} \rangle_{\text{p}}))} \overset{\hat{f} \to 0}{\sim} \frac{\nu^* \hat{f}}{5} \tag{60}$$

Therefore the point of divergence for the low force criteria is

$$\nu^* = \frac{5}{2\phi_2} \tag{61}$$

By applying Eq. (61) to the Marko and Siggia force-law we see that the low force criteria diverges at $\nu^* = 10/3$ as stated in Section 3.6. To calculate the divergence for the half-extension criteria, we set $\langle \hat{z}_{\text{tot}} \rangle_{\text{p}} = 1/2$ in Eq. (58) and substitute for $\hat{f}(1/2)$ from Eq. (26). The divergence is then given by the solution to

$$\frac{1}{2} = \frac{-3}{5\nu^*/4} + \frac{1}{\mathcal{L}(5\nu^*/4)} \tag{62}$$

which is $\nu^* = 2.4827$ as stated in Section 3.6.

It must be noted that while Eq. (58) is valid for any $0 < \langle \hat{z}_{\text{tot}} \rangle_{\text{p}} < 1$, and can be used for the low force criteria,

in general it *cannot* be used for the high force criteria. This stems from the break-down of the assumption in Eq. (48) if $\hat{f} \to \infty$, in particular because the spring potential for the WLC model diverges at full extension fast enough. In fact, we know that Eq. (58) cannot be valid for the WLC model for the high-force criterion because we know that the high force criteria does not diverge. It is shown in Section 5.1 that the high force criteria for the FENE model does diverge, and Eq. (58) *can* be used to calculate the position of divergence.

4. Rheological properties

Thus far we have only considered the force–extension behavior of the bead-spring chains. In addition to F–E behavior we are interested in the rheology of the bead-spring chains, and how it changes as the level of coarse-graining changes. In general, this is a much harder problem computationally than the work done thus far. In order to continue in the spirit of calculating properties near equilibrium and using equilibrium statistical mechanics, we will investigate the rheology of the bead-spring chains by looking at potential flow in the limit of small deformation rate. Potential flow has the desirable property that the chain behavior can be calculated using equilibrium statistical mechanics with an effective energy due to the flow. From this analysis the retarded-motion expansion coefficients can be calculated. These coefficients give insight into the rheological properties of the bead-spring chains in slow and slowly varying flows.

Thus the goal of this section is to examine the retarded-motion expansion coefficients for bead-spring chains. This has been done previously for Finitely Extensible Non-linear Elastic (FENE) [5] springs and for Hookean springs. Bird et al. [4] also present a general framework for the retarded-motion coefficients for any bead-spring-rod chain. However, because of the generality, that analysis cannot simplify the integrals over phase space to a convenient and intuitive form. Here we present the results of a specific application of that framework to only bead-spring chains but for arbitrary spring force-law. As assumed previously, we will assume that there are no bending potentials between springs and that the spring force only depends on the magnitude of extension. Furthermore we will neglect any hydrodynamic interaction and excluded volume between the beads and assume that the polymer solution is dilute. With these assumptions, the retarded-motion coefficients can be written as a function of simple moments of the force-law probability distribution. These moments are given by

$$\langle r^n \rangle_{\text{eq}} = \frac{\int_0^\ell \mathrm{d}r \, r^{n+2} \exp[-U_{\text{eff}}(r)/k_{\text{B}}T]}{\int_0^\ell \mathrm{d}r \, r^2 \exp[-U_{\text{eff}}(r)/k_{\text{B}}T]} \tag{63}$$

Written in terms of the moments, the first two retarded-motion expansion coefficients equal

$$b_1 - \eta_s = \eta_{0,p} = \frac{1}{36} n_p \zeta (N^2 - 1) \langle r^2 \rangle_{eq} \tag{64}$$

$$
\begin{aligned}
b_2 &= \frac{-\Psi_{1,0}}{2} \\
&= \left(\frac{-n_p \zeta^2}{120 k_B T} \right) \left[\left(\frac{\langle r^4 \rangle_{eq}}{15} - \frac{\langle r^2 \rangle_{eq}^2}{9} \right) \left(\frac{N^4 - 1}{N} \right) \right. \\
&\quad \left. + \left(\frac{\langle r^2 \rangle_{eq}^2}{9} \right) \left(\frac{(N^2 - 1)(2N^2 + 7)}{6} \right) \right]
\end{aligned} \tag{65}
$$

where η_s is the viscosity of the Newtonian solvent, $\eta_{0,p}$ the polymer contribution to the zero-shear viscosity, $\Psi_{1,0}$ the zero-shear first normal stress coefficient, n_p the number density of polymers, ζ the drag coefficient of each bead, and N the number of beads in the chain. Because we have neglected hydrodynamic interaction, we also know from Bird et al. [4] that b_{11} is zero. See Appendix B for the derivation of these coefficients. It should be emphasized that for Eqs. (64) and (65) *no assumption* has been made about the form of the spring force-law $U_{eff}(r)$.

A more common approach to calculating the polymer contribution to the zero-shear viscosity is through the Giesekus form of the stress tensor, from which it can be shown that

$$\eta_{0,p} = \frac{1}{6} n_p \zeta N R_g^2 \tag{66}$$

where R_g is the root mean square radius of gyration at equilibrium. For bead-spring chains R_g is related to the single spring moments as

$$R_g^2 = \frac{N^2 - 1}{6N} \langle r^2 \rangle_{eq} \tag{67}$$

From these equations we can verify Eq. (64). Eqs. (64), (65), and (67) were additionally used to calculate the model properties given in Tables 2–4 as discussed in Section 3.6. A relaxation time for the bead-spring chain can also be calculated from the retarded-motion expansion coefficients:

$$\tau_0 = \frac{-b_2}{b_1 - \eta_s} \tag{68}$$

Recalling from the definitions of the moments (Eq. (63)) that they are defined for a *single spring*, it seems natural to scale them by the fully extended length of a spring, ℓ, if it is finite. For that case let us define dimensionless moments as

$$\langle \hat{r}^n \rangle_{eq} = \frac{\langle r^n \rangle_{eq}}{\ell^n} = \frac{\int_0^1 d\hat{r} \, \hat{r}^{n+2} \, \exp[-(\nu/\lambda) \hat{U}_{eff}(\hat{r})]}{\int_0^1 d\hat{r} \, \hat{r}^2 \, \exp[-\nu/\lambda \hat{U}_{eff}(\hat{r})]} \tag{69}$$

After a number of parameter substitutions the retarded-motion expansion coefficients can be rewritten as

$$b_1 - \eta_s = \eta_{0,p} = \left(\frac{n_p (N\zeta) L A_{true}}{12} \right) \left(\frac{N+1}{N} \right) \left(\frac{\nu \langle \hat{r}^2 \rangle_{eq}}{3} \right) \tag{70}$$

$$
\begin{aligned}
b_2 &= \frac{-\Psi_{1,0}}{2} = \left(\frac{-n_p (N\zeta)^2 L^2 A_{true}^2}{120 k_B T} \right) \\
&\quad \times \left[\left(\frac{\nu^2 \langle \hat{r}^4 \rangle_{eq}}{15} - \frac{\nu^2 \langle \hat{r}^2 \rangle_{eq}^2}{9} \right) \left(\frac{(N^2 + 1)(N + 1)}{N^3 (N - 1)} \right) \right. \\
&\quad \left. + \left(\frac{\nu \langle \hat{r}^2 \rangle_{eq}}{3} \right)^2 \left(\frac{(N + 1)(2N^2 + 7)}{6N^2 (N - 1)} \right) \right]
\end{aligned} \tag{71}
$$

The advantage of working with the dimensionless moments is that they only depend on the parameters ν and λ but not on the absolute number of beads (or springs). Thus all dependence on the absolute number of beads is shown explicitly. In this way we have separated out in the formulae the contribution from the specific form of the spring force-law and the contribution from the chain having multiple beads. Contrary to the force–extension behavior, we do see a dependence on the absolute number of beads. The coefficients are made dimensionless as

$$\hat{\eta}_{0,p} = \frac{\eta_{0,p}}{n_p (N\zeta) L A_{true}/12} \tag{72}$$

$$\hat{b}_2 = \frac{b_2}{-n_p (N\zeta)^2 L^2 A_{true}^2/(120 k_B T)} \tag{73}$$

These were chosen as the scales because they depend only on properties intrinsic to the true polymer or the system of study. The polymer solution being modelled has a number density of polymers, n_p, and a temperature T. The true polymer being modelled has a value of the persistence length A_{true}, a contour length L, and a total drag. Because we are using a freely draining model, the total drag on the chain is $N\zeta$. By comparing dimensionless quantities with $N\zeta$ as the scale of drag, we are looking at how the property changes if for bead-spring models with different number of beads, we recalculate the drag on a single bead, ζ, such that the whole chain has a constant drag.

To better understand the behavior of the retarded-motion coefficients, let us first examine how much the coefficients depend explicitly on the number of beads (in addition to the level of coarse-graining, ν). In Figs. 12 and 13 we show respectively $\hat{\eta}_{0,p}$ and $\hat{b}_2$ as a function of the number of beads, N, while the level of coarse-graining, ν, is held constant. The $\hat{\eta}_{0,p}$ curves for different values of ν are exactly self-similar as could be seen from Eq. (70), while the $\hat{b}_2$ curves are approximately self-similar except when both ν and N are small. We attribute the change of the coefficients with N while ν is held fixed to the fact that for finite N the drag is not distributed along a continuous contour. Thus for the bead-spring model to be an accurate coarse-grained model of the true polymer, the number of beads must be large enough to operate in the large N region. The deviation for $\nu < \infty$ is due to the errors in the spring force-law as discussed in Section 3 with regards to the F–E behavior. The $\nu = \infty$ curve corresponds to the
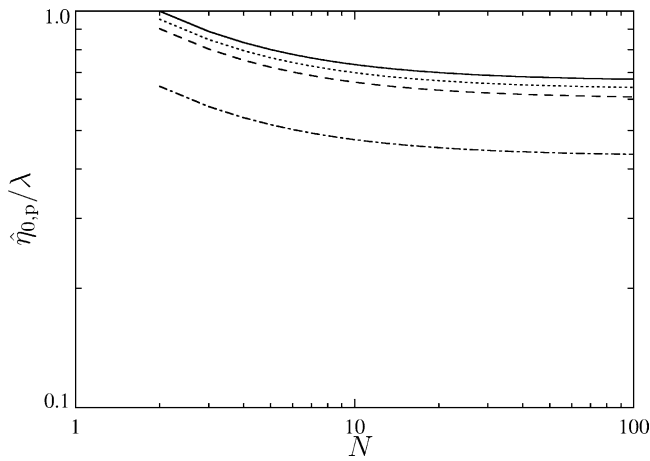
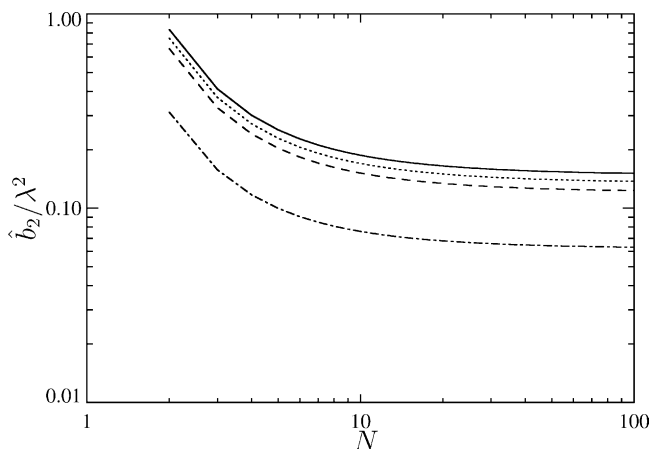Fig. 12. Polymer contribution to the zero-shear viscosity of Marko and Siggia bead-spring chains as the number of effective persistence lengths represented by each spring, ν/λ, is held constant. The curves correspond to $\nu/\lambda = \infty$ (solid line), $\nu/\lambda = 400$ (dotted), $\nu/\lambda = 100$ (dashed), and $\nu/\lambda = 10$ (dash-dot).
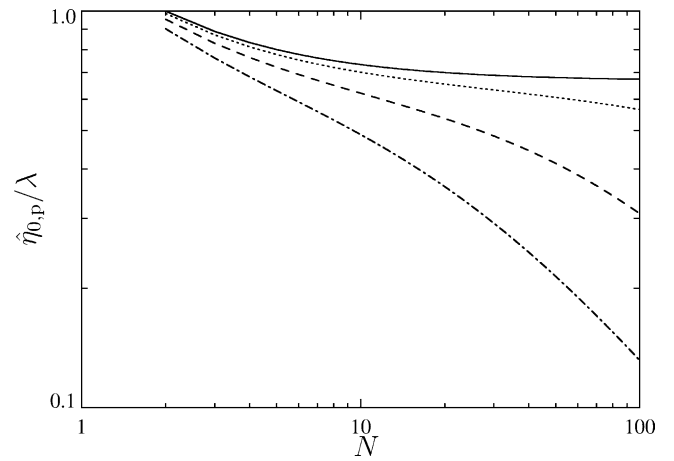

Fig. 14. Polymer contribution to the zero-shear viscosity of Marko and Siggia bead-spring chains as the number of effective persistence lengths in the total polymer contour, α/λ, is held constant. The curves correspond to $\alpha/\lambda = \infty$ (solid line), $\alpha/\lambda = 4000$ (dotted), $\alpha/\lambda = 400$ (dashed), and $\alpha/\lambda = 100$ (dash-dot).

"Rouse model" result. What we mean by the "Rouse model" result will be discussed later.

In order to model a given polymer with different numbers of beads, the value of ν is not constant. Instead the value of α (the number of true persistence lengths in the polymer's contour) is constant. In Figs. 14 and 15 we show respectively $\hat{\eta}_{0,p}$ and $\hat{b}_2$ as a function of the number of beads, N, while α is held constant. This corresponds to discretizing a polymer finer and finer. We can see the interplay between drag error and discretizing error as discussed in the introduction. When the number of beads is small, error is present because the drag on the polymer due to the solvent is lumped at the beads, not exerted along a continuous contour. When the number of beads is large, error is present because the polymer has been discretized so finely that each spring represents a small number of persistence lengths. As discussed previously this

fine discretization leads to error predicting the size of the coil and the extension of polymer segments. If the number of persistence lengths in the whole polymer, α, is large enough, there exists an approximate plateau. This corresponds to the situation in which the number of springs is simultaneously large enough to reduce the drag error and small enough to prevent discretization error. Using the expansions developed in Section 3.8 we can *predict* the location of this plateau.

To use these expansions and also explain why the behavior approaches the "Rouse result", we need to express the spring moments in terms of the force–extension behavior. From Eq. (39) we see that

$$\lim_{\hat{f} \to 0} \left(\frac{\partial}{\partial \hat{f}} \langle \hat{z}_{tot} \rangle_m \right) = \frac{\nu \langle \hat{r}^2 \rangle_{eq}}{3} \qquad (74)$$

Fig. 13. Zero-shear first normal stress coefficient of Marko and Siggia bead-spring chains as the number of effective persistence lengths represented by each spring, ν/λ, is held constant. The curves correspond to $\nu/\lambda = \infty$ (solid line), $\nu/\lambda = 400$ (dotted), $\nu/\lambda = 100$ (dashed), and $\nu/\lambda = 10$ (dash-dot).
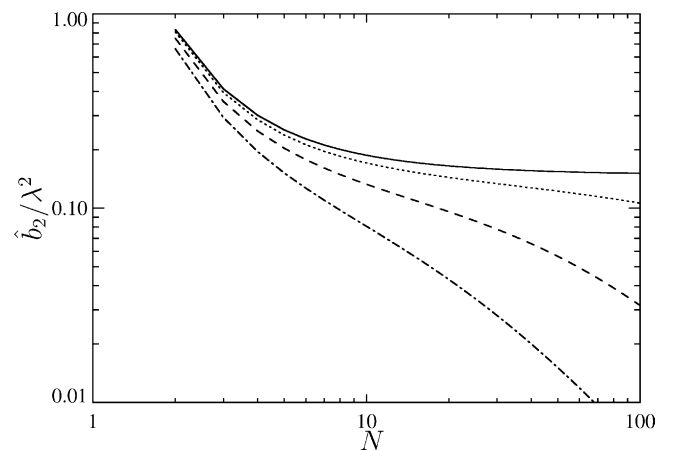

Fig. 15. Zero-shear first normal stress coefficient of Marko and Siggia bead-spring chains as the number of effective persistence lengths in the total polymer contour, α/λ, is held constant. The curves correspond to $\alpha/\lambda = \infty$ (solid line), $\alpha/\lambda = 4000$ (dotted), $\alpha/\lambda = 400$ (dashed), and $\alpha/\lambda = 100$ (dash-dot).

It can also be shown by taking the third derivative of the force–extension curve that

$$\frac{1}{3\nu} \lim_{\hat{f}\to 0} \left(\frac{\partial^3}{\partial \hat{f}^3} \langle \hat{z}_{tot} \rangle_m \right) = \frac{\nu^2 \langle \hat{r}^4 \rangle_{eq}}{15} - \frac{\nu^2 \langle \hat{r}^2 \rangle_{eq}^2}{9} \qquad (75)$$

Making use of these equalities we can write the retarded-motion expansion coefficients as

$$\hat{\eta}_{0,p} = \left(\frac{N+1}{N} \right) \left(\lim_{\hat{f}\to 0} \frac{\partial}{\partial \hat{f}} \langle \hat{z}_{tot} \rangle_m \right) \qquad (76)$$

$$\hat{b}_2 = \left[\left(\frac{1}{3\nu} \lim_{\hat{f}\to 0} \frac{\partial^3}{\partial \hat{f}^3} \langle \hat{z}_{tot} \rangle_m \right) \left(\frac{(N^2+1)(N+1)}{N^3(N-1)} \right) \right.$$
$$\left. + \left(\lim_{\hat{f}\to 0} \frac{\partial}{\partial \hat{f}} \langle \hat{z}_{tot} \rangle_m \right)^2 \left(\frac{(N+1)(2N^2+7)}{6N^2(N-1)} \right) \right] \qquad (77)$$

Let us first examine the plateau of $\hat{\eta}_{0,p}$. We can easily see from the pre-factor in Eq. (76) that the drag error is negligible if

$$N \gg 1 \qquad (78)$$

To predict the upper limit of the plateau, we use the expansion in Eq. (44). Use of this series is justified because we know that if the behavior is within the plateau region then ν must be very large. In fact, the leading order term must be dominant. For the WLC model this corresponds to

$$|d_1| \left(\frac{\lambda}{\nu\phi_2} \right)^{1/2} \ll 1 \qquad (79)$$

Written in terms of the parameter α/λ, which is constant while discretizing, this condition becomes

$$(N-1)^{1/2} \ll \frac{1}{|d_1|} \left(\frac{\alpha\phi_2}{\lambda} \right)^{1/2} \qquad (80)$$

Note that this is true for the WLC model because for the Marko and Siggia spring potential

$$\phi_2 = \frac{3}{4}, \qquad d_1 = \frac{-4}{3\sqrt{\pi}} \qquad (81)$$

However some models like the FENE model have $d_1 = 0$. The appropriate analysis shows that in general

$$(N-1)^{i/2} \ll \frac{1}{|d_i|} \left(\frac{\alpha\phi_2}{\lambda} \right)^{i/2} \qquad (82)$$

where i denotes the first coefficient d_i that is non-zero (excluding $d_0 = 1$). Combining the two bounds on N gives a formula for the plateau region for $\hat{\eta}_{0,p}$:

$$1 \ll N, \quad (N-1)^{i/2} \ll \frac{1}{|d_i|} \left(\frac{\alpha\phi_2}{\lambda} \right)^{i/2} \qquad (83)$$

A similar analysis can be done for $\hat{b}_2$. Because α has to be large for a plateau region to even exist, we will neglect

the term with the third derivative. Following an analogous procedure we find the plateau region for $\hat{b}_2$:

$$2 \ll N, \quad (N-1)^{i/2} \ll \frac{1}{|2d_i|} \left(\frac{\alpha\phi_2}{\lambda} \right)^{i/2} \qquad (84)$$

Note the factors of two that result from expanding the rational function of N for large N and from expanding the square of the zero-force slope.

Let us consider application of these formulae to the WLC model. For the Marko and Siggia potential with $\lambda = 1$ the two plateau conditions state that

$$1 \ll N, \quad (N-1)^{1/2} \ll 1.151\alpha^{1/2} \qquad (85)$$

$$2 \ll N, \quad (N-1)^{1/2} \ll 0.576\alpha^{1/2} \qquad (86)$$

If we consider that an order of magnitude difference is sufficient to satisfy the $\ll$ conditions, then the conditions could be approximated as

$$15 \lesssim N \lesssim 0.01\alpha \qquad (87)$$

In words this says that the number of beads must be larger than approximately 15 while simultaneously each spring must represent more than approximately 100 persistence lengths. Recall that based on force–extension simulations [19] of the Kramers chain, Somasi et al. [14] argued than each spring should represent more than 10 Kuhn lengths but were not able to estimate a lower bound on the number of springs and had to extrapolate from the Kramers chain result to the WLC result. Here we have used zero Weissenberg rheology to derive *both* lower and upper bounds on the number of beads for arbitrary spring force-law. From Brownian dynamics simulations of start-up of steady shear flow [14], there is initial evidence that our bounds may even retain approximate validity in unsteady, strong flows. We leave a detailed analysis of this to future research.

In addition to allowing for the derivation of the plateau region, writing b_1 and b_2 in terms of the force–extension curve allows for a better physical understanding for the deviation of the curves for $\nu < \infty$ and what is meant by the "Rouse result". The "Rouse result" is the value that the Rouse model would give if the spring constant were equated to the zero-extension slope of the *spring* force-law. Recalling that the *spring* force-law was taken from the *true polymer* force–extension behavior, one can show that this Rouse model would have coefficients

$$\hat{\eta}_{0,p} = \left(\frac{N+1}{N} \right) \left(\lim_{\hat{f}\to 0} \frac{\partial}{\partial \hat{f}} \langle \hat{z}_{tot} \rangle_p \right) \qquad (88)$$

$$\hat{b}_2 = \left[\left(\lim_{\hat{f}\to 0} \frac{\partial}{\partial \hat{f}} \langle \hat{z}_{tot} \rangle_p \right)^2 \left(\frac{(N+1)(2N^2+7)}{6N^2(N-1)} \right) \right] \qquad (89)$$

We see that because the force–extension behavior of the model approaches that of the true polymer as $\nu \to \infty$, the retarded-motion expansion coefficients of the model approach the Rouse result. Note that while the part of b_2 with the

third derivative is zero for the Rouse result because its spring is Hookean, that term vanishes for the model as $\nu \to \infty$ because of the $1/\nu$ pre-factor. The third derivative of the true polymer force–extension curve is *not* zero.

Now we turn to a discussion of how using a best-fit λ criteria affects the rheological behavior as the polymer is more finely discretized. In particular let us look more closely at the low-force criteria. The low-force criteria is such that

$$\lim_{\hat{f} \to 0} \frac{\partial}{\partial \hat{f}} \langle \hat{z}_{\text{tot}} \rangle_{\text{m}} = \lim_{\hat{f} \to 0} \frac{\partial}{\partial \hat{f}} \langle \hat{z}_{\text{tot}} \rangle_{\text{p}} \tag{90}$$

If we put this result into Eqs. (76) and (77) we see that the zero-shear viscosity equals the Rouse result exactly. The zero-shear first normal stress coefficient will be close to the Rouse result but will deviate slightly. This is because the third derivative is non-zero and ν is not infinite. Note that the third derivative is also not equal to the third derivative of the true polymer force–extension curve. The equality and approximate equality with the Rouse results holds only up to a critical N, at which point the low-force criterion diverges (Eq. (61)):

$$N_{\text{max}} = \tfrac{2}{5}\phi_2 \alpha + 1 \tag{91}$$

5. Examples of other force-laws

Thus far whenever a particular spring force-law has been needed the Marko and Siggia interpolation formula has been used. It has been noted that the general formula will work for other force laws. Here we will explicitly show how the formulae can be made specific for two important force-laws commonly used in modelling polymer rheology.

5.1. FENE force-law

The first force-law we will consider is the FENE force-law, which is a widely used approximation to the behavior of a freely jointed chain (FJC). The FENE force-law can be written in general as

$$f = \frac{H\ell \langle \hat{z}_{\text{tot}} \rangle_{\text{p}}}{1 - \langle \hat{z}_{\text{tot}} \rangle_{\text{p}}^2} \tag{92}$$

In the sense that the FENE force-law is an approximation to the true force-law for a FJC, the spring constant H is given in terms of the length of a rod in the FJC, or Kuhn length a_{K}, as [4]

$$H = \frac{3k_{\text{B}}T}{\ell a_{\text{K}}} \tag{93}$$

Combining Eqs. (92) and (93), the appropriate scale for the force is $k_{\text{B}}T/a_{\text{K}}$, or for the general case $H\ell$. The general formalism presented earlier scaled the force by $k_{\text{B}}T/A_{\text{true}}$ where A_{true} was called the true persistence length. Now it is clear that it would be more appropriate to call A_{true} a generalized flexibility length, and only for the WLC is it equal to the

"persistence length". For the FJC the generalized flexibility length is proportional to the Kuhn length.

To apply the framework presented in Section 3 to the FENE force-law in Eq. (92), we will let $A_{\text{true}} = k_{\text{B}}T/(H_{\text{true}}\ell) = a_{\text{K,true}}/3$ so that the "exact" polymer F–E behavior is

$$\hat{f} = \frac{\langle \hat{z}_{\text{tot}} \rangle_{\text{p}}}{1 - \langle \hat{z}_{\text{tot}} \rangle_{\text{p}}^2} \tag{94}$$

This directly motivates the choice for the spring force-law

$$f_{\text{spring}}(r) = \left(\frac{k_{\text{B}}T}{A_{\text{eff}}} \right) \frac{r/\ell}{1 - (r/\ell)^2} \tag{95}$$

where A_{eff} is defined in the expected way as

$$A_{\text{eff}} = \frac{k_{\text{B}}T}{H_{\text{eff}}\ell} = \frac{a_{\text{K,eff}}}{3} \tag{96}$$

It is then clear that the dimensionless energy for the FENE spring becomes

$$\hat{U}_{\text{eff}}(\hat{r}) = \frac{-1}{2}\ln(1 - \hat{r}^2) \tag{97}$$

and all formulae from Section 3 follow directly. However, while interpreting the previous discussion it must be kept in mind that the parameters dependent on A_{eff} and A_{true} can have slightly different physical interpretations depending on the exact force-law used. What does not change is the concept that those parameters consist of generalized flexibility lengths. Thus, for example, ν still must be large in order for the bead-spring model to behave like the true polymer.

For the FENE force-law many of the calculations (integrals) can be performed analytically. In particular, the F–E behavior is

$$\langle \hat{z}_{\text{tot}} \rangle_{\text{m}} = \frac{I_{k+1}(\hat{f}\nu)}{I_k(\hat{f}\nu)}, \quad k = \frac{3 + \nu/\lambda}{2} \tag{98}$$

where $I_k(x)$ is the modified Bessel function of the first kind, order k. The moments can also be calculated analytically in terms of the Beta function, or equivalently Gamma functions:

$$\langle \hat{r}^n \rangle_{\text{eq}} = \frac{\Gamma((n+3)/2)}{\Gamma(3/2)} \frac{\Gamma(3/2 + \nu/(2\lambda) + 1)}{\Gamma(((n+3)/2) + \nu/(2\lambda) + 1)} \tag{99}$$

For even values of $n \geq 2$, they take an even simpler form:

$$\langle \hat{r}^n \rangle_{\text{eq}} = \frac{(n+1)(n-1)\cdots(3)}{(n+3+\nu/\lambda)(n+1+\nu/\lambda)\cdots(5+\nu/\lambda)} \tag{100}$$

In order to more easily compare these results with the large body of literature on FENE springs, we will relate the common FENE notation to the notation used here. Typically the FENE force-law is written as [4]

$$f_{\text{lit}}(Q) = \frac{H_{\text{lit}}Q}{1 - (Q/Q_o)^2} \tag{101}$$

Comparing Eqs. (95) and (101) we see the following equalities in notation:

$$Q \rightarrow r \tag{102}$$

$$Q_o \rightarrow \ell \tag{103}$$

$$H_{\text{lit}} \rightarrow H_{\text{eff}} \tag{104}$$

The other very important parameter in the FENE notation is b defined by

$$b = \frac{H_{\text{lit}} Q_o^2}{k_B T} \tag{105}$$

which can be related to our notation as

$$b \rightarrow \frac{\nu}{\lambda} \tag{106}$$

For comparison with the WLC results presented thus far, we here present the corresponding results for the FENE model. In Fig. 16 we show the F–E behavior of FENE bead-spring chains as the level of coarse-graining, ν, is changed. We see that the FENE result is qualitatively similar to the WLC result in Fig. 3.

For the FENE force-law λ can also be taken greater than one to obtain a better behavior from the model. Fig. 17 shows the "best-fit" λ versus $1/\nu$ for each of the three criteria introduced in Section 3.6. The most obvious difference from the WLC result in Fig. 5 is that for the FENE chain the high-force criterion curve deviates from $\lambda = 1$. In fact, the high-force criterion curve diverges similar to the other criteria. We will see that this high-force divergence is because of the weaker divergence of the FENE force-law approaching full extension compared to the WLC force-law. This divergence of the high-force criteria also causes the best fit λ curves to form a relatively narrow strip bounding the choices for λ. In Fig. 18

Fig. 17. Calculation of λ for the three different criteria at different levels of coarse-graining for the FENE potential. The criteria shown are low-force (dash-dot), half-extension (dashed), and high-force (dotted). Inset: Expanded view showing the divergence of the criteria.

we compare the force–extension behavior of the three criteria for $\nu = 20$. While we see a qualitative match for the relative error with the Marko and Siggia result (Fig. 6), the error is greatly reduced. Thus for the FENE force-law simply adjusting the effective flexibility length does a much better job at reproducing the true polymer behavior over the entire force range. This is due to the form of the high-extension divergence of the force-law. The trade-off for this improved performance is that the range in ν that this correction-factor can be used is reduced.

The high-force and low-force best-fit λ curves can be calculated exactly. Recall that the low-force criterion is that the slope at zero force matches the true polymer slope. Using Eq. (39) for the slope, and using Eq. (100) for the second
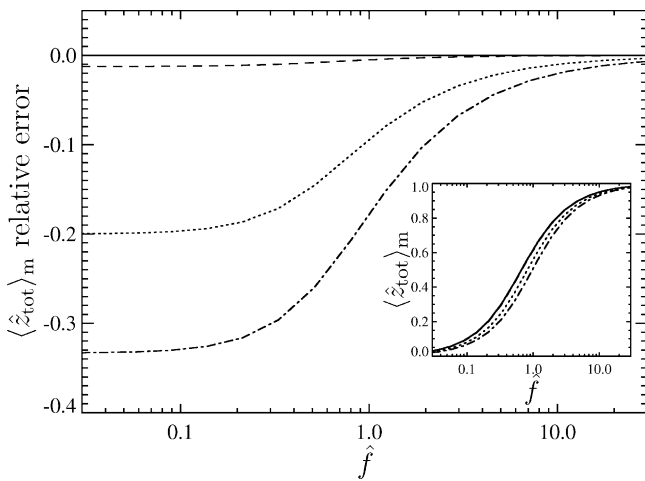

Fig. 16. Calculation of the relative error of the mean fractional extension, $(\langle \hat{z}_{\text{tot}} \rangle_m - \langle \hat{z}_{\text{tot}} \rangle_p)/\langle \hat{z}_{\text{tot}} \rangle_p$, for a bead-spring model as the level of coarse-graining changes. The FENE potential was used with $\lambda = 1$. The curves correspond to $\nu = 400$ (dashed), $\nu = 20$ (dotted), and $\nu = 10$ (dash-dot). Inset: the mean fractional extension of the models compared with the "true polymer" (solid line, Eq. (94)).
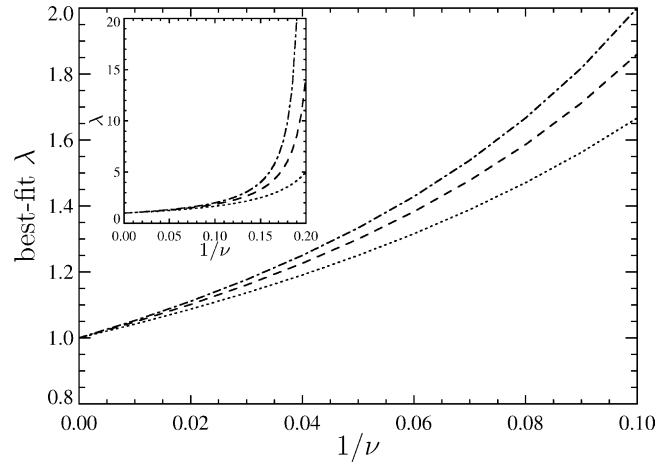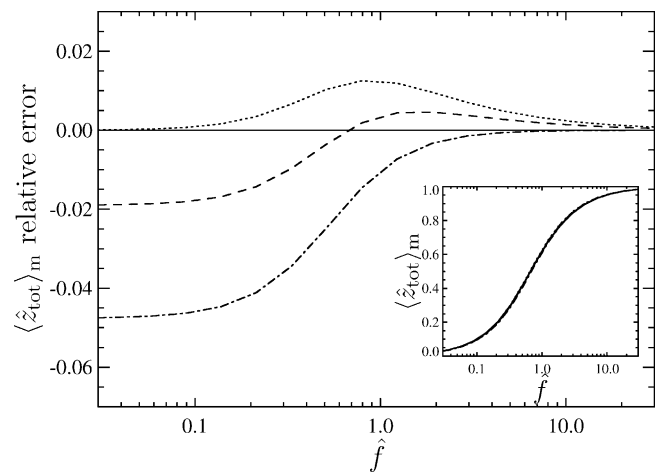

Fig. 18. Calculation of the relative error of the mean fractional extension, $(\langle \hat{z}_{\text{tot}} \rangle_m - \langle \hat{z}_{\text{tot}} \rangle_p)/\langle \hat{z}_{\text{tot}} \rangle_p$, for a bead-spring model for different best fit criteria. The FENE potential was used with $\nu = 20$. The curves correspond to $\lambda = 1.33$ (low-force, dotted), $\lambda = 1.30$ (half-extension, dashed), and $\lambda = 1.25$ (high-force, dash-dot). Inset: the mean fractional extension of the models compared with the "true polymer" (solid line, Eq. (94)).

moment, we find that the low-force criteria curve is given by

$$\lambda = \frac{1}{1 - 5/\nu} \tag{107}$$

from which it is easy to see the curve diverges at $\nu^* = 5$. This could also have been seen from the general low-force divergence formula in Eq. (61) since $\phi_2 = 1/2$ for the FENE force-law. The high-force curve is calculated from the high-force expansion of the fractional extension:

$$\langle \hat{z}_{\text{tot}} \rangle_m \overset{\hat{f} \to \infty}{\sim} 1 - \frac{\nu/\lambda + 4}{2\nu \hat{f}} + O\left(\frac{1}{\hat{f}^2}\right) \tag{108}$$

Since the true polymer has a high-force expansion of

$$\langle \hat{z}_{\text{tot}} \rangle_p \overset{\hat{f} \to \infty}{\sim} 1 - \frac{1}{2\hat{f}} + O\left(\frac{1}{\hat{f}^2}\right) \tag{109}$$

the high-force criteria curve is given by

$$\lambda = \frac{1}{1 - 4/\nu} \tag{110}$$

with a divergence at $\nu^* = 4$. This can also be derived from the general divergence criteria in Eq. (58). By comparing the expansion

$$\frac{-3}{\nu^* \hat{f}(\langle \hat{z}_{\text{tot}} \rangle_p)} + \frac{1}{\mathcal{L}(\nu^* \hat{f}(\langle \hat{z}_{\text{tot}} \rangle_p))} \overset{\hat{f} \to \infty}{\sim} 1 - \frac{2}{\nu^* \hat{f}} \tag{111}$$

with the expansion of the true polymer, we can verify that the high-force criteria diverges at $\nu^* = 4$. The half-extension divergence is found by solving the equation

$$\frac{1}{2} = \frac{-3}{2\nu^*/3} + \frac{1}{\mathcal{L}(2\nu^*/3)} \tag{112}$$

which has a solution $\nu^* = 4.6551$.

In addition to the F–E behavior of the FENE chains, we should look at the fluctuations, as done for the WLC in Section 3.7. In Figs. 19 and 20 we show the plots of the scaled root-mean-squared fluctuations for different levels of coarse-graining, ν. From the high-force expansion of the FENE force–extension behavior in Eq. (108) we can calculate the high-force scaling of the fluctuations:

$$\alpha^{1/2} \delta \hat{z} \overset{\hat{f} \to \infty}{\sim} \left(\frac{\nu/\lambda + 4}{2\nu}\right)^{1/2} \frac{1}{\hat{f}} + O\left(\frac{1}{\hat{f}^2}\right) \tag{113}$$

$$\alpha^{1/2} \delta \hat{x} \overset{\hat{f} \to \infty}{\sim} \frac{1}{\hat{f}^{1/2}} + O\left(\frac{1}{\hat{f}^{3/2}}\right) \tag{114}$$

We can also analyze the limiting behavior from Section 3.8 in terms of the FENE force-law. Because the FENE force-law is an odd function of its argument, the general expansion of the F–E behavior in the large ν limit can additionally be used at zero force. We can examine in detail the expansion of the zero-force slope (Eq. (39)) because the zero-force slope can
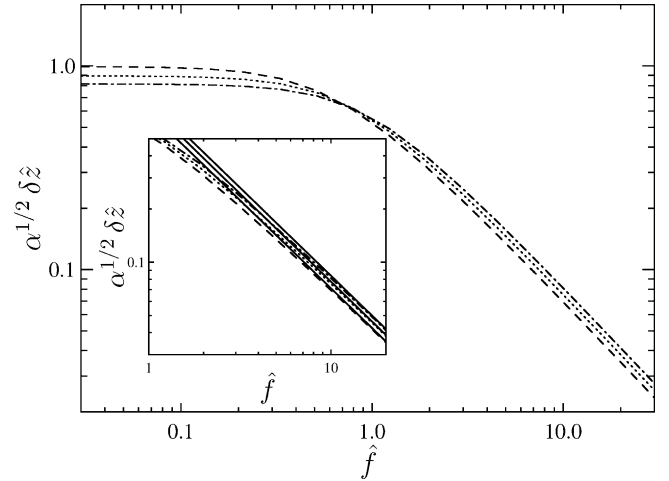

Fig. 19. Calculation of the longitudinal root-mean-squared fluctuations at different levels of coarse-graining. The FENE potential was used with $\lambda = 1$. The curves correspond to $\nu = 400$ (dashed), $\nu = 20$ (dotted), and $\nu = 10$ (dash-dot). Inset: detailed look at the high-force limit with solid lines corresponding to the asymptotic behavior, $((\nu/\lambda + 4)/(2\nu))^{1/2}(1/\hat{f})$.

be calculated exactly. Using the expression for the second moment of the FENE force-law,

$$\lim_{\hat{f} \to 0} \left(\frac{\partial}{\partial \hat{f}} \langle \hat{z}_{\text{tot}} \rangle_m\right) = \frac{\nu}{5 + \nu/\lambda} \tag{115}$$

We see that the expansion of this slope for large ν should just be the Taylor expansion. Calculating the coefficients, d_i, using the FENE force-law shows this explicitly. The parameters of the FENE force-law are

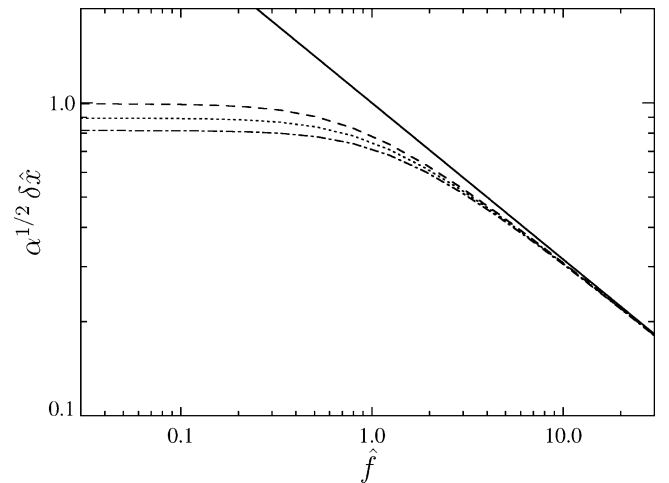$$\phi_2 = \tfrac{1}{2} \tag{116}$$

Fig. 20. Calculation of the transverse root-mean-squared fluctuations at different levels of coarse-graining. The FENE potential was used with $\lambda = 1$. The curves correspond to $\nu = 400$ (dashed), $\nu = 20$ (dotted), and $\nu = 10$ (dash-dot). The solid line corresponds to the high-force asymptotic behavior, $1/(\hat{f}^{1/2})$.

$$h_i = \begin{cases} 0, & i \text{ even} \\ \dfrac{1}{i+3}, & i \text{ odd} \end{cases} \tag{117}$$

which gives coefficients

$$d_i = \begin{cases} 0, & i \text{ odd} \\ \left(\dfrac{-5}{2}\right)^{i/2}, & i \text{ even} \end{cases} \tag{118}$$

Since this is the geometric series, the convergence is well-known. Note also that the zero-one Padé $P_1^0(1/\nu)$ gives the exact result.

Because we have simple formulae for the moments of the FENE force-law, the retarded-motion expansion coefficients reduce to simple formulae. In fact, they correctly reduce to the previous result by Wiest and Tanner [5]:

$$\hat{\eta}_{0,p} = \left(\frac{N+1}{N}\right)\left(\frac{\nu}{\nu/\lambda + 5}\right) \tag{119}$$

$$\hat{b}_2 = \frac{\nu^2(N+1)}{6(\nu/\lambda + 5)^2(N-1)N^2}\left[\frac{-12(N^2+1)}{N(\nu/\lambda + 7)} + 2N^2 + 7\right] \tag{120}$$

We can apply the same methodology used to analyze the zero Weissenberg number rheology of the WLC to the FENE bead-spring chain. Figs. 21 and 22 show the first two retarded-motion expansion coefficients when the level of coarse-graining, ν, is held constant. Figs. 23 and 24 show the coefficients as the polymer is discretized finer and finer. We see the same qualitative trends as with the WLC coefficients. If the number of beads is small, there is error in the rheology due to the drag being exerted only at the beads, instead of along a continuous contour. However, if the polymer is being more finely discretized, then there is error if the polymer is

Fig. 22. Zero-shear first normal stress coefficient of FENE bead-spring chains as the number of effective persistence lengths represented by each spring, ν/λ, is held constant. The curves correspond to $\nu/\lambda = \infty$ (solid line), $\nu/\lambda = 400$ (dotted), $\nu/\lambda = 100$ (dashed), and $\nu/\lambda = 10$ (dash-dot).

discretized too finely. This is due to error in representing the size of the coil and the extension of polymer segments.

5.2. Infinitely stiff Fraenkel force-law/FJC

The other force-law we consider explicitly is the infinitely stiff Fraenkel force-law, which is equivalent to the FJC. This force-law differs from the others considered because the spring potential *is not* obtained by examining the force–extension behavior of a true polymer. In fact, this force-law *is* a model of a "true polymer" (the FJC or random walk model). Thus the previous discussions of the comparison between the bead-spring model and the true polymer do not apply for this force-law. However, we can still use the formulae developed to calculate the F–E and rheological behavior of this true polymer.
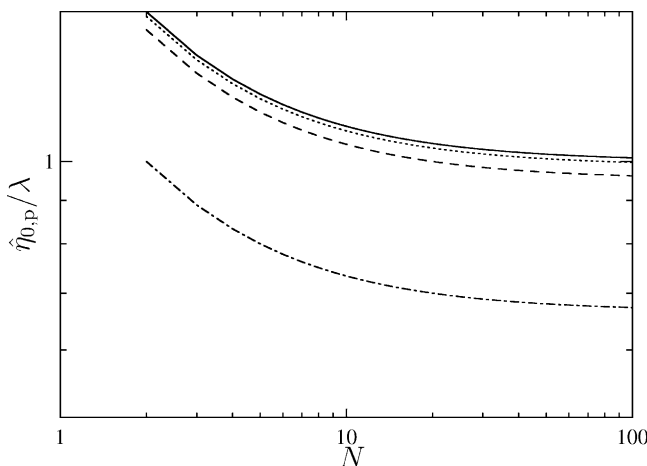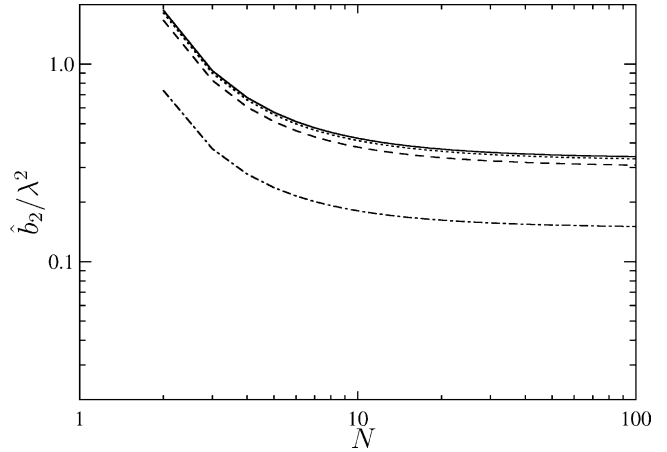

Fig. 21. Polymer contribution to the zero-shear viscosity of FENE bead-spring chains as the number of effective persistence lengths represented by each spring, ν/λ, is held constant. The curves correspond to $\nu/\lambda = \infty$ (solid line), $\nu/\lambda = 400$ (dotted), $\nu/\lambda = 100$ (dashed), and $\nu/\lambda = 10$ (dash-dot).
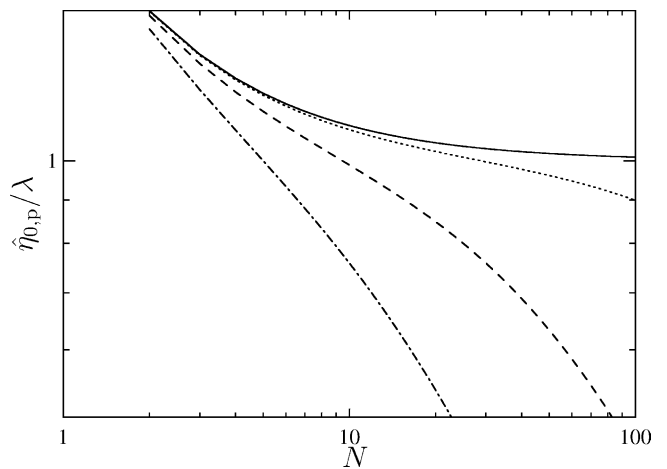

Fig. 23. Polymer contribution to the zero-shear viscosity of FENE bead-spring chains as the number of effective persistence lengths in the total polymer contour, α/λ, is held constant. The curves correspond to $\alpha/\lambda = \infty$ (solid line), $\alpha/\lambda = 4000$ (dotted), $\alpha/\lambda = 400$ (dashed), and $\alpha/\lambda = 100$ (dash-dot).
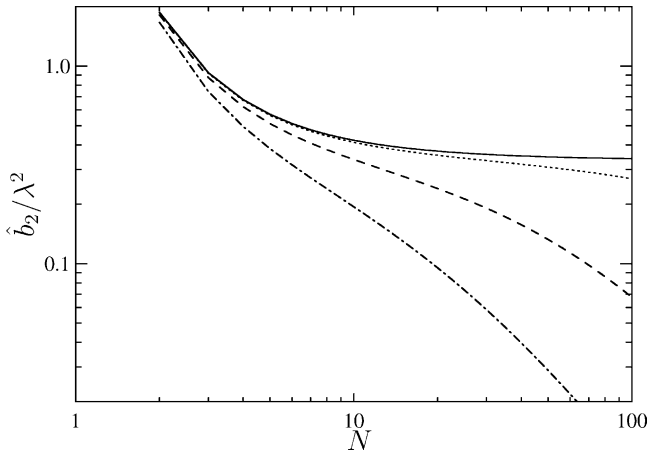
Fig. 24. Zero-shear first normal stress coefficient of FENE bead-spring chains as the number of effective persistence lengths in the total polymer contour, α/λ, is held constant. The curves correspond to $\alpha/\lambda = \infty$ (solid line), $\alpha/\lambda = 4000$ (dotted), $\alpha/\lambda = 400$ (dashed), and $\alpha/\lambda = 100$ (dash-dot).

The Fraenkel force-law is a Hookean force-law, but with a minimum energy at a non-zero extension:

$$f_{\text{spring}}(r) = H_{\text{F}}(r - a_{\text{K}}) \tag{121}$$

H_{F} is the spring constant of the Fraenkel spring, and a_{K} is the position of minimum energy. We use the symbol a_{K} because for the infinitely stiff Fraenkel spring this minimum corresponds to the Kuhn length in the FJC. After integrating, the spring potential becomes

$$U_{\text{eff}}(r) = \tfrac{1}{2} H_{\text{F}}(r - a_{\text{K}})^2 \tag{122}$$

For the infinitely stiff model, $H_{\text{F}} \to \infty$, the Boltzmann factor becomes a Dirac delta function:

$$\exp\left[\frac{-U_{\text{eff}}(r)}{k_{\text{B}}T} \right] \to \delta(r - a_{\text{K}}) \tag{123}$$

Furthermore, in this limit the contour length of the model, L, becomes $N_s a_{\text{K}}$, so the length of a spring, ℓ, becomes a_{K}. Since the choice of A_{true} is arbitrary, we will take it to be the Kuhn length, a_{K}. Thus in dimensionless form

$$\exp\left[\frac{-\nu}{\lambda} \hat{U}_{\text{eff}}(\hat{r}) \right] \to \delta(\hat{r} - 1) \tag{124}$$

$$\nu = 1 \tag{125}$$

Using these expressions in Eq. (25) for the F–E behavior, we see that

$$\langle \hat{z}_{\text{tot}} \rangle_{\text{m}} = \left\{ \frac{-1}{\hat{f}} + \frac{\partial}{\partial \hat{f}} \ln \left(\int_0^1 d\hat{r}\, \hat{r}\, \sinh\left[\hat{f}\hat{r} \right] \delta(\hat{r} - 1) \right) \right\}$$

$$= \mathcal{L}\left(\hat{f} \right) \tag{126}$$

which we already know is the F–E behavior of the FJC. Note that this is the F–E behavior for *any* integer number of springs (Kuhn lengths). Even a *single* rod of a FJC has the Langevin function for its F–E behavior. Also note that for the Fraenkel

spring force-law, the upper limit of integration should be ∞ instead of 1. However, for the infinitely stiff case, replacing the ∞ by 1 causes no change to the F–E behavior.

To calculate the rheological properties, as in Section 4, we need to calculate the moments, which are

$$\langle \hat{r}^n \rangle_{\text{eq}} = 1 \tag{127}$$

The first two retarded-motion expansion coefficients then become

$$\hat{\eta}_{0,\text{p}} = \frac{N+1}{3N} \tag{128}$$

$$\hat{b}_2 = \frac{N+1}{54N^2(N-1)} \left[\frac{-12(N^2+1)}{5N} + 2N^2 + 7 \right] \tag{129}$$

which are the well-known results for the infinitely stiff Fraenkel chain (equivalent to the FJC) [4]. By taking the ratio of the two coefficients, we can calculate a relaxation time for the chain:

$$\tau_0 = \frac{\Psi_{1,0}}{2\eta_{0,\text{p}}} = \frac{\zeta a_{\text{K}}^2}{180\, k_{\text{B}}T} \left[\frac{-12(N^2+1)}{5N} + 2N^2 + 7 \right] \tag{130}$$

6. Polymer Ensemble Transformation method

Recall that previously the spring force-law was chosen by examining the force–extension behavior of the true polymer in the constant force ensemble, as shown in Sections 3.4 and 5.1. The mean fractional z-projection of the polymer was replaced by the fractional radial coordinate of the spring. In this section we examine a new method for determining the spring force-law, which we term the Polymer Ensemble Transformation (PET) method. This method uses the constant extension behavior of the true polymer to determine the spring force-law. The bead-spring model is then able to reproduce the behavior of the true polymer in both the constant extension and constant force ensembles. Reproducing the behavior in the constant force ensemble is critical because we saw in Section 4 that the retarded-motion coefficients can be written in terms of the force–extension behavior in the constant force ensemble.

6.1. Physical interpretation

The method of using the constant extension ensemble behavior to obtain a spring force-law is illustrated in Fig. 25. In the figure, a polymer is shown in the constant force ensemble. The goal is to determine a spring force-law that can model the polymer behavior at a given set of reference points (depicted by black circles in the figure), while coarse-graining out the details of the polymer between the reference points. To accomplish this, the segment of polymer to be modelled is placed in the constant extension ensemble, and the average external force required to keep the polymer at a fixed extension is calculated. The spring force in the model is taken to
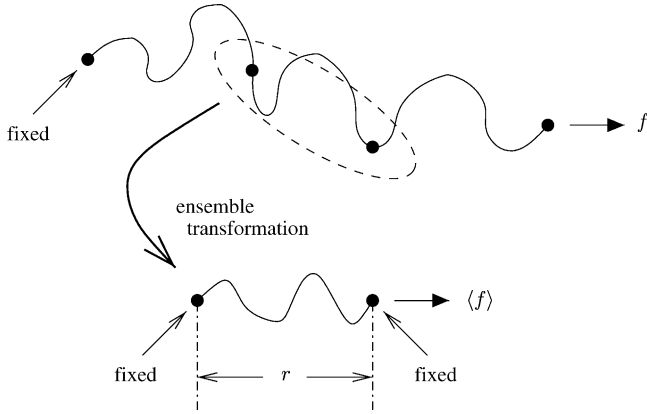
Fig. 25. Physical interpretation of Polymer Ensemble Transformation (PET) method. Above: the true polymer in the constant force ensemble. The behavior is to be modelled between reference points (black circles). Below: the portion of true polymer between reference points is transformed to the constant extension ensemble to calculate the appropriate spring force-law.

be equal to this average force:

$$f_{\text{spring}}(r) = \langle f \rangle(r) \tag{131}$$

If the reference points on the true polymer correspond to free hinges (as in the FJC with the reference points taken at the joints), then the spring model defined in this way reproduces exactly the force–extension behavior of the true polymer. However, for other polymers such as the WLC, there is coupling across the reference points. Therefore this preliminary bead-spring model cannot reproduce the true polymer behavior for this class of polymers. We believe that this error can be approximately accounted for by introducing bending potentials between springs, however leave this topic for future research.

6.2. Mathematical justification

To derive that the spring force-law *must* be taken from the constant extension ensemble in order to reproduce the force–extension behavior in the constant force ensemble, we start by writing down the partition function in the constant force ensemble

$$\mathcal{Z}(\boldsymbol{f}) = \int \cdots \int_{\{\text{configurations}\}} \exp\left[\frac{-U + \boldsymbol{f} \cdot \mathbf{R}_{\text{tot}}}{k_{\text{B}}T}\right] d\mathbb{V} \tag{132}$$

where the force has not necessarily been taken to lie in the *z*-direction. We can introduce a new variable, $\boldsymbol{r}$, through the use of a Dirac delta function:

$$\mathcal{Z}(\boldsymbol{f}) = \int \cdots \int_{\{\text{configurations}\}} \exp\left[\frac{-U + \boldsymbol{f} \cdot \mathbf{R}_{\text{tot}}}{k_{\text{B}}T}\right]$$
$$\times \int \delta(\boldsymbol{r} - \mathbf{R}_{\text{tot}}) \, d\boldsymbol{r} \, d\mathbb{V} \tag{133}$$

By interchanging the order of integration, we obtain

$$\mathcal{Z}(\boldsymbol{f}) = \int \int \cdots \int_{\{\text{configurations}\}}$$
$$\times \exp\left[\frac{-U + \boldsymbol{f} \cdot \mathbf{R}_{\text{tot}}}{k_{\text{B}}T}\right] \delta(\boldsymbol{r} - \mathbf{R}_{\text{tot}}) \, d\mathbb{V} d\boldsymbol{r} \tag{134}$$

The force term can be taken out of the configuration integral because of the delta function so that

$$\mathcal{Z}(\boldsymbol{f}) = \int \Omega(\boldsymbol{r}) \exp\left[\frac{\boldsymbol{f} \cdot \boldsymbol{r}}{k_{\text{B}}T}\right] d\boldsymbol{r} \tag{135}$$

where

$$\Omega(\boldsymbol{r}) = \int \cdots \int_{\{\text{configurations}\}} \exp\left[\frac{-U}{k_{\text{B}}T}\right] \delta(\boldsymbol{r} - \mathbf{R}_{\text{tot}}) d\mathbb{V} \tag{136}$$

is the constant extension ensemble partition function. However, we see that this looks similar to the partition function of a single dumbbell model:

$$\mathcal{Z}(\boldsymbol{f}) = \int \exp\left[\frac{-U_{\text{s}}(\boldsymbol{r})}{k_{\text{B}}T}\right] \exp\left[\frac{\boldsymbol{f} \cdot \boldsymbol{r}}{k_{\text{B}}T}\right] d\boldsymbol{r} \tag{137}$$

Thus a single dumbbell model will have the exact same partition function as the true polymer (and thus the exact same equilibrium behavior) if the spring potential energy is taken from the constant extension partition function as

$$U_{\text{s}}(\boldsymbol{r}) = -k_{\text{B}}T \ln \Omega(\boldsymbol{r}) \tag{138}$$

Here we illustrated how the spring potential can be derived for a single dumbbell. However, a similar procedure can be used to derive bead-spring chains. All of the spring coordinates can be introduced into the partition function by using Dirac delta functions (as in Eq. (133)). For example, if three springs were desired the transformation would give

$$\mathcal{Z}(\boldsymbol{f}) = \int \Omega(\boldsymbol{r}_1, \boldsymbol{r}_2, \boldsymbol{r}_3) \exp\left[\frac{\boldsymbol{f} \cdot (\boldsymbol{r}_1 + \boldsymbol{r}_2 + \boldsymbol{r}_3)}{k_{\text{B}}T}\right]$$
$$\times d\boldsymbol{r}_1 d\boldsymbol{r}_2 d\boldsymbol{r}_3 \tag{139}$$

where $\boldsymbol{r}_i$ is the spring connector vector of spring i. The potential energy of the spring system would then be

$$U_{\text{s}}(\boldsymbol{r}_1, \boldsymbol{r}_2, \boldsymbol{r}_3) = -k_{\text{B}}T \ln \Omega(\boldsymbol{r}_1, \boldsymbol{r}_2, \boldsymbol{r}_3) \tag{140}$$

Note that the total potential energy of the spring system is in general not separable into contributions from each spring, and thus includes coupling between springs.

We saw in Eq. (135) how the constant force and constant extension partition function are related. This is exactly analogous to the relationship between the microcanonical and canonical ensembles, as well as between other ensembles [23,33]. If we look at the analytic continuation of the constant force partition function onto the imaginary force axis,

we find that it is the Fourier transform of the constant extension partition function:

$$\mathcal{Z}(ik_{\mathrm B}T\boldsymbol{k}) = \int \Omega(\boldsymbol{r}) \exp\left[i\boldsymbol{k} \cdot \boldsymbol{r}\right] \mathrm{d}\boldsymbol{r} \tag{141}$$

Thus, the constant extension ensemble partition function can be calculated from the constant force ensemble partition function as

$$\Omega(\boldsymbol{r}) = \left(\frac{1}{2\pi}\right)^d \int \mathcal{Z}(ik_{\mathrm B}T\boldsymbol{k}) \exp\left[-i\boldsymbol{k} \cdot \boldsymbol{r}\right] \mathrm{d}\boldsymbol{k} \tag{142}$$

where d is the dimensionality of the vectors. This means that there is a one-to-one correspondence between the two partition functions. If we produce a bead-spring chain with the same constant force ensemble partition function as the true polymer, then necessarily it has the same constant extension ensemble partition function as the true polymer. Though this is obvious for a single dumbbell model, it is not obvious for a multiple spring chain.

6.3. Application to FJC/Random Walk Spring model

As an example of this new method, we apply it to the freely jointed chain model. The result, which we call the Random Walk Spring (RWS) model, is a set of spring forces that allow for the modelling of a FJC with a bead-spring chain at *any* level of discretization while still reproducing the entire force–extension behavior.

We have seen in the previous sections that in order to model the FJC with a bead-spring chain, we must choose the spring potential from the constant extension ensemble partition function. This can be calculated from Eq. (136) directly for the FJC by taking the Fourier transform of both sides, and then inverting the transform. Alternatively, the partition function can be calculated from Eq. (142) since the constant force ensemble partition function is known. The methods obviously give the same result, which is that the constant extension ensemble partition function is proportional to the probability density of a three dimensional random walk, given by the well-known Rayleigh's formula [4]. If the generalized flexibility length is taken to be the Kuhn length, $A_{\mathrm{true}} = a_{\mathrm K}$, then ν corresponds to the number of Kuhn lengths represented by each spring. In our notation the constant force ensemble partition function using Rayleigh's formula is

$$\Omega(r) = \frac{1}{r} \int_0^\infty u \sin(ur) \left[\frac{\sin(uA_{\mathrm{true}})}{uA_{\mathrm{true}}}\right]^\nu \mathrm{d}u \tag{143}$$

where the integral represents an inverse Fourier transform. We can therefore write the spring potential energy in the Random Walk Spring model, valid for integer ν, as

$$U_{\mathrm s}(r) = -k_{\mathrm B}T \ln\left\{\frac{1}{r} \int_0^\infty u \sin(ur) \left[\frac{\sin(uA_{\mathrm{true}})}{uA_{\mathrm{true}}}\right]^\nu \mathrm{d}u\right\} \tag{144}$$

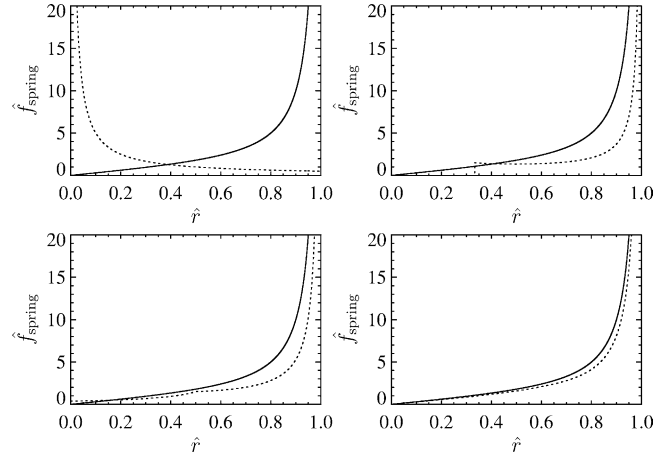Fig. 26. Comparison of the spring force-law chosen from the Random Walk Spring (RWS) model (dotted) and chosen from the constant force ensemble force–extension behavior of the true polymer (the inverse Langevin function, solid line). The spring force is plotted as $\hat{f}_{\mathrm{spring}} = f_{\mathrm{spring}}A_{\mathrm{true}}/k_{\mathrm B}T$. The different plots correspond to $\nu = 2$ (upper left), $\nu = 3$ (upper right), $\nu = 4$ (lower left), and $\nu = 10$ (lower right).

The spring force is calculated as the derivative of the spring potential:

$$f_{\mathrm{spring}}(r) = -k_{\mathrm B}T$$
$$\times \frac{\partial}{\partial r} \ln\left\{\frac{1}{r} \int_0^\infty u \sin(ur) \left[\frac{\sin(uA_{\mathrm{true}})}{uA_{\mathrm{true}}}\right]^\nu \mathrm{d}u\right\} \tag{145}$$

By construction this model reproduces *exactly* the force–extension behavior of the FJC for integer ν. In Fig. 26 we compare this spring force-law with the inverse Langevin function for different values of ν. For $\nu = 2$ we see the RWS force-law increasing with decreasing extension, and even diverging at zero extension, but also with a discontinuous divergence at full extension to prevent over-extension. By performing the integration for $\nu = 2$ it is easy to show

$$f_{\mathrm{spring}} = \frac{k_{\mathrm B}T}{r}, \quad r < \ell \tag{146}$$

We also show in Appendix C how one can verify that this force-law gives the required F–E behavior of the FJC. For $\nu = 3$ the RWS model produces another interesting force-law. Up to one-third extension, the force is zero. At one-third extension, the force discontinuously jumps to a finite value. The force-law decreases to a minimum then increases up to a divergence at full extension. The functional form for the case of $\nu = 3$ is

$$f_{\mathrm{spring}} = \frac{3k_{\mathrm B}TA_{\mathrm{true}}}{(3A_{\mathrm{true}} - r)r}, \quad \frac{\ell}{3} < r < \ell \tag{147}$$

For $\nu > 3$ the RWS model spring force-laws are continuous. However, $\nu = 4$ still shows notable characteristics. At half extension this force-law has a discontinuous first derivative, and the force has a non-zero limit at zero extension. This

force-law is given by

$$
f_{\text{spring}} = \begin{cases} \dfrac{3k_{\text{B}}T}{8A_{\text{true}} - 3r}, & 0 < r < \dfrac{\ell}{2} \\[2ex] \dfrac{k_{\text{B}}T(4A_{\text{true}} + r)}{(4A_{\text{true}} - r)r}, & \dfrac{\ell}{2} < r < \ell \end{cases} \tag{148}
$$

Recall that the inverse Langevin function is the constant force ensemble force–extension behavior of the true polymer. Therefore, the inverse Langevin function would be the spring force-law used in the "conventional" method of using the constant force ensemble to obtain the spring force-law. The differences between the RWS model and the inverse Langevin function illustrate why the "conventional" method cannot be used to model short segments of the FJC (small ν). Only for $\nu \to \infty$ are the constant force and constant extension ensembles equivalent, in which case the inverse Langevin function becomes the correct spring force-law.

6.4. Implementation of model

There exist some issues concerning the implementation of models derived from the PET method that warrant mentioning. First, the PET method can produce spring force-laws that are discontinuous. This presents no problem for analytic techniques such as statistical mechanics. However, if the spring force-laws are implemented in techniques such as Brownian dynamics, very steep force-laws must be used to accurately represent the needed discontinuity. This is the case for the RWS model if ν equals one, two, or three. Note however that the $\nu = 1$ case is in fact the case of an infinitely stiff Fraenkel spring. This case, including the use of a corrective potential force, has been discussed previously [25].

Second, the use of the PET method requires the force–extension curve for the finite-length polymer of interest. This was trivial for the FJC case, but is not trivial for models such as the WLC. Only recently have calculations been performed of the force–extension behavior of finite-length worm-like chains [34,35].

Finally, we consider a little closer the possible coupling across reference points in Fig. 25 (depicted by black circles). While we leave a detailed analysis for future research, we consider two limits here for the case of the worm-like chain. In the limit of an infinite number of persistence lengths between each reference point, we know that no bending potential is needed. In the limit of zero persistence lengths between each reference point, the polymer acts like a rigid rod. In this limit a bending potential of

$$
U_{\text{bend}}(\theta) = \frac{k_{\text{B}}TA_{\text{true}}}{2\ell}\theta^2 \tag{149}
$$

where θ is the angle between rods and ℓ the length of a rod gives the exact WLC model. Note that this bending energy could also be used in the limit of an infinite number of persistence lengths between reference points because in that limit, $A_{\text{true}}/\ell \to 0$, we recover the needed absence of bending energy. At intermediate levels of discretization for models such as the WLC, a simple bending potential may also be able to reproduce the true polymer behavior. It should be noted these issues of coupling and bending potentials do not occur in the single dumbbell model, and the PET method always reproduces the true polymer behavior.

7. Conclusion

In this paper we have used statistical mechanics to systematically analyze the coarse-graining of polymers into bead-spring chains. In this way we could avoid the intrinsic stochastic noise of Brownian dynamics, identify the relevant dimensionless groups, and examine limiting and universal behavior. We began by studying the force–extension behavior of the bead-spring chains. The analysis was then continued to rheological behavior by examining the retarded-motion expansion coefficients, which describe the zero Weissenberg number response. We then introduced a new method for coarse-graining called the Polymer Ensemble Transformation (PET) method which uses the constant extension ensemble to determine the spring force-law.

The analysis of the force–extension behavior revealed that, because the springs are decoupled, the response depended only on the number of flexibility lengths represented by each spring, ν. This necessarily means that any deviation between the behavior of the spring model and the true polymer cannot be due to the number of free hinges introduced. Instead we showed through direct visualization of the phase space that ν acts analogously to an inverse temperature, controlling the magnitude of fluctuations in phase space.

We also examined quantitatively the use of an effective flexibility length to partially correct the force–extension behavior. The corrected curve is not uniformly valid over the entire force range leading to multiple possible choices for the effective flexibility length. However, we were able to place bounds on the choices and examine these choices. Variability in behavior within these bounds depends on the form of the spring force-law; the Marko and Siggia potential has larger variability than the FENE potential. This is mainly due to the difference in the divergence of the potentials at high extension.

To study the zero Weissenberg number rheology we calculated the first two retarded-motion expansion coefficients for bead-spring chains with *arbitrary* spring force-law. The contribution due to the spring force-law was separated from the contribution due to the number of springs chained together. In contrast to the force–extension behavior the zero Weissenberg number rheology illustrates a dependence on the number of beads even if the number of flexibility lengths per spring is held constant. We attribute this error to the drag being exerted only on the beads, instead of along a continuous contour. A plateau region in which both the drag error and discretization error are small was identified, and the position and size of that plateau were *predicted*.

Finally, we reexamined how the *form* of the spring potential is chosen. The Polymer Ensemble Transformation (PET) method was introduced and justified. This new method for coarse-graining polymers into bead-spring chains uses the force–extension behavior of the true polymer in the constant extension ensemble as the spring force-law. It is shown that this method can give the exact force–extension behavior for arbitrary level of discretization. *There is nothing intrinsically incorrect about using springs to model short segments of a polymer.* The conventional spring force-laws fail at high discretization because they are taken from the constant force ensemble. The two ensembles are only equivalent if the polymer has an infinite number of flexibility lengths. The PET method was applied to the freely jointed chain polymer, resulting in the Random Walk Spring (RWS) model. The RWS model is a set of spring force-laws that can exactly model the force–extension behavior of the freely jointed chain at any level of discretization.

With this work we have begun along the path towards a rigorous understanding of coarse-graining, with particular application to modelling polymers with bead-spring chains. It has not escaped our notice that the analysis presented here could be continued to study coarse-graining in transient, strong flows and to consider excluded volume and hydrodynamic interactions.

Acknowledgements

Appendix A. Fluctuations in force–extension behavior

This Appendix discusses the derivation of the fluctuations in the force–extension behavior for bead-spring chains, Eqs. (34) and (35). Recall that the average extension of the chain is calculated as

$$\langle z_{\text{tot}} \rangle = \frac{1}{\mathcal{Z}_{\text{w}}} \underbrace{\int \cdots \int}_{\{\text{configurations}\}} z_{\text{tot}} \exp\left[\frac{-U + f z_{\text{tot}}}{k_B T}\right] d\mathbb{V} \quad (A.1)$$

Using the quotient rule, the derivative with respect to the force can be calculated:

$$\frac{\partial}{\partial f} \langle z_{\text{tot}} \rangle = \frac{1}{k_B T} \langle (z_{\text{tot}} - \langle z_{\text{tot}} \rangle)^2 \rangle \quad (A.2)$$

Non-dimensionalizing gives the desired result for the longitudinal fluctuations.

The transverse fluctuations are calculated by writing down explicitly the prescribed average. We first note that

$$\langle x_{\text{tot}}^2 \rangle = N_s \langle x^2 \rangle \quad (A.3)$$

where x is the x-coordinate of a single spring because all the cross-terms between springs vanish. The average over the single spring is

$$\langle x^2 \rangle = \frac{1}{\mathcal{Z}_s} \int x^2 \exp\left[\frac{-U_s(r) + fz}{k_B T}\right] d^3 r \quad (A.4)$$

We then write the integral explicitly in spherical coordinates:

$$\langle x^2 \rangle = \frac{1}{\mathcal{Z}_s} \int r^4 \cos^2 \phi \, \sin^3 \theta \, \exp\left[\frac{-U_s(r) + fr\cos\theta}{k_B T}\right]$$
$$\times \, dr \, d\theta \, d\phi \quad (A.5)$$

We can rewrite the ϕ-integral using the relation

$$\int_0^{2\pi} \cos^2 \phi \, d\phi = \pi = \frac{1}{2} \int_0^{2\pi} d\phi \quad (A.6)$$

We can rewrite the θ-integral by integrating by parts once:

$$\int_0^\pi \sin^3 \theta \, \exp\left[\frac{fr\cos\theta}{k_B T}\right] d\theta$$
$$= \frac{2k_B T}{fr} \int_0^\pi \sin\theta \, \cos\theta \, \exp\left[\frac{fr\cos\theta}{k_B T}\right] d\theta \quad (A.7)$$

Using these relations we see that

$$\langle x^2 \rangle = \frac{k_B T}{f \mathcal{Z}_s} \int r^3 \cos\theta \, \sin\theta$$
$$\times \exp\left[\frac{-U_s(r) + fr\cos\theta}{k_B T}\right] dr \, d\theta \, d\phi \quad (A.8)$$

The resulting integral is simply the average z-coordinate of a single spring:

$$\langle x^2 \rangle = \frac{k_B T}{f} \langle z \rangle \quad (A.9)$$

The z-coordinate of the whole chain is given by

$$\langle z_{\text{tot}} \rangle = N_s \langle z \rangle \quad (A.10)$$

which combined with Eq. (A.9) gives the transverse fluctuation for the whole chain:

$$\langle x_{\text{tot}}^2 \rangle = \frac{k_B T}{f} \langle z_{\text{tot}} \rangle \quad (A.11)$$

Non-dimensionalizing gives the desired result for the transverse fluctuations.

Appendix B. Retarded-motion expansion coefficients

This Appendix discusses the derivation of the retarded-motion coefficients for bead-spring chains, Eqs. (64) and (65). This is a specific application of the general bead-spring-rod chain framework of Bird et al. [4]. The analysis is similar

to the FENE chain result by Wiest and Tanner [5], but is much more general because it does not assume a form for the spring force-law.

We consider the behavior of the bead-spring chains in steady, homogenous potential flow for which the velocity gradient tensor, κ, is symmetric and constant. In this case, the chain probability density function is given by the equilibrium statistical mechanics result with an effective energy due to the flow [4] :

$$\psi = \frac{1}{J} \exp\left[\frac{\zeta}{2k_B T} \sum_{jk} C_{jk}\kappa : r_j r_k - \frac{U}{k_B T}\right] \tag{B.1}$$

In this expression, the matrix C_{jk} is a symmetric $(N-1) \times (N-1)$ matrix called the Kramers matrix and is given by

$$C_{jk} = \begin{cases} \frac{j(N-k)}{N}, & j \le k \\ \frac{k(N-j)}{N}, & k \le j \end{cases} \tag{B.2}$$

the vector r_j represents the connector vector of spring j, U is the total potential energy of the springs, and

$$J = \int \exp\left[\frac{\zeta}{2k_B T} \sum_{jk} C_{jk}\kappa : r_j r_k - \frac{U}{k_B T}\right] dr^{N-1} \tag{B.3}$$

Note that sums over roman indices are from 1 to $(N-1)$. We can rewrite the probability density in terms of the equilibrium $(\kappa = 0)$ values:

$$\psi = \psi_{eq} \frac{J_{eq}}{J} \exp\left[\frac{\zeta}{2k_B T} \sum_{jk} C_{jk}\kappa : r_j r_k\right] \tag{B.4}$$

$$\psi_{eq} = \frac{1}{J_{eq}} \exp\left[\frac{-U}{k_B T}\right] \tag{B.5}$$

$$J_{eq} = \int \exp\left[\frac{-U}{k_B T}\right] dr^{N-1} \tag{B.6}$$

We now expand ψ in the limit of small κ. In order to expand the ratio J_{eq}/J, we make use of the relation

$$\langle r_j r_k \rangle_{eq} = \delta_{jk} \frac{1}{3} \langle r^2 \rangle_{eq} \delta \tag{B.7}$$

where r_j represents the magnitude of the vector r_j and we have dropped the subscript within the average since the average does not depend on the value of the subscript. Furthermore, for an incompressible fluid

$$\kappa : \delta = \text{tr}\kappa = 0 \tag{B.8}$$

Using these relations, the probability density function to first order is

$$\psi = \psi_{eq} \left\{1 + \frac{\zeta}{2k_B T} \sum_{jk} C_{jk}\kappa : r_j r_k\right\} \tag{B.9}$$

To use this probability density function to calculate the rheological behavior we use the non-equilibrium part of the stress tensor in Giesekus form:

$$\tau = -2\eta_s\kappa + \tau_p \tag{B.10}$$

$$\tau_p = \frac{-n_p\zeta}{2}\left\{\kappa \cdot \left\langle \sum_{ij} C_{ij} r_i r_j \right\rangle + \left\langle \sum_{ij} C_{ij} r_i r_j \right\rangle \cdot \kappa\right\} \tag{B.11}$$

The probability density function in Eq. (B.9) is used to perform the prescribed averages and obtain the stress tensor up to second order in κ. To write the expression for the stress tensor in terms of moments of the spring force distribution, it must be used that

$$\langle r_i r_j r_m r_k \rangle_{eq} = \delta_{ij}\delta_{jm}\delta_{mk}\frac{1}{15}\langle r^4 \rangle_{eq}(\delta\delta + I + I^\dagger),$$

$$-\delta_{ij}\delta_{mk}(\delta_{jm} - 1)\frac{1}{9}\langle r^2 \rangle_{eq}^2\delta\delta,$$

$$-\delta_{im}\delta_{jk}(\delta_{jm} - 1)\frac{1}{9}\langle r^2 \rangle_{eq}^2 I^\dagger,$$

$$-\delta_{ik}\delta_{jm}(\delta_{ji} - 1)\frac{1}{9}\langle r^2 \rangle_{eq}^2 I \tag{B.12}$$

where I and $I^\dagger$ are fourth-order isotropic tensors defined with Cartesian components [4]

$$I_{mnpq} = \delta_{mq}\delta_{np}, \qquad I^\dagger_{mnpq} = \delta_{mp}\delta_{nq} \tag{B.13}$$

Relations involving the sum over the Kramers matrix must also be used:

$$\sum_i C_{ii} = \frac{N^2 - 1}{6}, \qquad \sum_i C_{ii}^2 = \frac{N^4 - 1}{30N},$$

$$\sum_{ij} C_{ij}^2 = \frac{(N^2 - 1)(2N^2 + 7)}{180} \tag{B.14}$$

Using these relations and performing the averages in the stress tensor we find that up to second order in κ

$$\tau = -2\left\{\eta_s + \frac{n_p\zeta(N^2 - 1)}{36}\langle r^2 \rangle_{eq}\right\}\kappa$$

$$-\frac{n_p\zeta^2}{k_B T}\left[\left(\frac{\langle r^4 \rangle_{eq}}{15} - \frac{\langle r^2 \rangle_{eq}^2}{9}\right)\left(\frac{N^4 - 1}{30N}\right)\right.$$

$$\left. + \left(\frac{\langle r^2 \rangle_{eq}^2}{9}\right)\left(\frac{(N^2 - 1)(2N^2 + 7)}{180}\right)\right]\kappa \cdot \kappa \tag{B.15}$$

However, the retarded-motion expansion can also be used to calculate the stress tensor in steady, homogeneous potential flow up to second order in κ, for which

$$\tau = -2b_1\kappa + 4b_2\kappa \cdot \kappa - 4b_{11}\kappa \cdot \kappa \tag{B.16}$$

Additionally we know from Bird et al. [4] that because we are considering bead-spring chains which do not have rigid

constraints and we have neglected hydrodynamic interaction, b_{11} is zero. Thus, from matching Eqs. (B.15) and (B.16) we find the desired formulae for the retarded-motion expansion coefficients in terms of the moments of the spring force distribution.

Appendix C. Example of the behavior of the Random Walk Spring model

This Appendix discusses how one can calculate the behavior of the Random Walk Spring (RWS) model for $\nu = 2$ and verify that it correctly models the freely jointed chain. Thus, we want to calculate the force–extension behavior in the constant force ensemble of a bead-spring chain with

$$f_{\text{spring}}(r) = \frac{k_B T}{r}, \quad r < \ell, \ \nu = 2 \tag{C.1}$$

This is done using the methodology presented in Section 3.4 and shown in Eq. (25). By integrating the spring force-law, and choosing a convenient arbitrary additive constant, we find that

$$U_{\text{eff}}(r) = k_B T \ln\left(\frac{r}{\ell}\right) \tag{C.2}$$

This gives a Boltzmann factor of

$$\exp\left[\frac{-\nu}{\lambda} \hat{U}_{\text{eff}}(\hat{r})\right] = \exp\left[-\ln(\hat{r})\right] = \frac{1}{\hat{r}} \tag{C.3}$$

and a corresponding mean extension of

$$\langle \hat{z}_{\text{tot}} \rangle_m = \frac{1}{2}\left\{ \frac{-1}{\hat{f}} + \frac{\partial}{\partial \hat{f}} \ln\left(\int_0^1 d\hat{r}\, \sinh[2\hat{f}\hat{r}]\right)\right\} \tag{C.4}$$

After performing the integration of the hyperbolic sine, the mean fractional extension becomes

$$\langle \hat{z}_{\text{tot}} \rangle_m = \frac{1}{2}\left\{ \frac{-1}{\hat{f}} + \frac{\partial}{\partial \hat{f}} \ln\left(\frac{\cosh(2\hat{f})}{2\hat{f}} - \frac{1}{2\hat{f}}\right)\right\} \tag{C.5}$$

$$\langle \hat{z}_{\text{tot}} \rangle_m = \frac{1}{2}\left\{ \frac{-2}{\hat{f}} + \frac{2\sinh(2\hat{f})}{\cosh(2\hat{f}) - 1}\right\} \tag{C.6}$$

By making use of trigonometric identities, we can simplify this expression to

$$\langle \hat{z}_{\text{tot}} \rangle_m = \frac{-1}{\hat{f}} + \frac{2\sinh(\hat{f})\cosh(\hat{f})}{2\sinh^2(\hat{f})} = \mathcal{L}(\hat{f}) \tag{C.7}$$

This example has illustrated how to use a spring force-law from the RWS model. In particular, we have shown explicitly that if one wants to model a freely jointed chain with each spring representing two Kuhn lengths ($\nu = 2$), one should choose the spring force-law shown in Eq. (146) because it has a force–extension behavior equal to the Langevin function.

References

[1] P.J. Flory, Statistical Mechanics of Chain Molecules, Oxford University Press, New York, 1989.

[2] W.L. Mattice, U.W. Suter, Conformational Theory of Large Molecules, Wiley Interscience, New York, 1994.

[3] W. Kuhn, F. Grun, Relationships between elastic constants and stretching double refraction of highly elastic substances, Kolloid Z. 101 (1942) 248.

[4] R.B. Bird, C.F. Curtiss, R.C. Armstrong, O. Hassager, Dynamics of polymeric liquids, in: Kinetic Theory, vol. 2, 2nd ed., Wiley, New York, 1987.

[5] J.M. Wiest, R.I. Tanner, Rheology of bead-nonlinear spring chain macromolecules, J. Rheol. 33 (2) (1989) 281–316.

[6] B.H.A.A. van den Brule, Brownian dynamics simulation of finitely extensible bead-spring chains, J. Non-Newton. Fluid. Mech. 47 (1993) 357–378.

[7] P.S. Doyle, E.S.G. Shaqfeh, Dynamic simulation of freely draining, flexible bead-rod chains: start-up of extensional and shear flow, J. Non-Newton. Fluid. Mech. 76 (1998) 43–78.

[8] J.S. Hur, E.S.G. Shaqfeh, R.G. Larson, Brownian dynamics simulations of single DNA molecules in shear flow, J. Rheol. 44 (4) (2000) 713–742.

[9] O. Kratky, G. Porod, X-ray investigation of dissolved chain molecules, Recl. Trav. Chim. 68 (1949) 1022–1106.

[10] J.F. Marko, E.D. Siggia, Stretching DNA, Macromolecules 28 (26) (1995) 8759–8770.

[11] H.R. Warner, Kinetic theory and rheology of dilute suspensions of finitely extendible dumbbells, Ind. Eng. Chem. Fundam. 11 (1972) 379–387.

[12] A. Cohen, A Padé approximant to the inverse Langevin function, Rheol. Acta 30 (1991) 270–272.

[13] L.E. Wedgewood, D.N. Ostrov, R.B. Bird, A finitely extensible bead-spring chain model for dilute polymer solutions, J. Non-Newton. Fluid. Mech. 40 (1991) 119–139.

[14] M. Somasi, B. Khomami, N.J. Woo, J.S. Hur, E.S.G. Shaqfeh, Brownian dynamics simulations of bead-rod and bead-spring chains: numerical algorithms and coarse-graining issues, J. Non-Newton. Fluid. Mech. 108 (2002) 227–255.

[15] I. Ghosh, G.H. McKinley, R.A. Brown, R.C. Armstrong, Deficiencies of FENE dumbbell models in describing the rapid stretching of dilute polymer solutions, J. Rheol. 45 (3) (2001) 721–758.

[16] R.G. Larson, T.T. Perkins, D.E. Smith, S. Chu, Hydrodynamics of a DNA molecule in a flow field, Phys. Rev. E 55 (2) (1997) 1794–1797.

[17] R.G. Larson, H. Hu, D.E. Smith, S. Chu, Brownian dynamics simulations of a DNA molecule in an extensional flow field, J. Rheol. 43 (2) (1999) 267–304.

[18] R.G. Larson, T.T. Perkins, D.E. Smith, S. Chu, Flexible Polymer Chains in Elongational Flow: Theory and Experiment, Springer, New York, 1999, Chapter 9.

[19] P.S. Doyle, E.S.G. Shaqfeh, A.P. Gast, Dynamic simulation of freely draining flexible polymers in steady linear flows, J. Fluid. Mech. 334 (1997) 251–291.

[20] P.S. Doyle, B. Ladoux, J.-L. Viovy, Dynamics of a tethered polymer in shear flow, Phys. Rev. Lett. 84 (20) (2000) 4769–4772.

[21] J.M. Deutsch, Theoretical studies of DNA during gel electrophoresis, Science 240 (1988) 922–924.

[22] J. Chuang, Y. Kantor, M. Kardar, Anomalous dynamics of translocation, Phys. Rev. E 65 (2001) 011802.

[23] R.K. Pathria, Statistical Mechanics, 2nd ed., Butterworths-Heinemann, Boston, 1996.

[24] H.C. Öttinger, Stochastic Processes in Polymeric Fluids: Tools and Examples for Developing Simulation Algorithms, Springer, Berlin, 1996.

[25] P.S. Grassia, E.J. Hinch, L.C. Nitsche, Computer simulations of Brownian motion of complex systems, J. Fluid Mech. 282 (1995) 373–403.

[26] R.M. Jendrejack, J.J. de Pablo, M.D. Graham, Stochastic simulations of DNA in flow: dynamics and the effects of hydrodynamic interactions, J. Chem. Phys. 116 (17) (2002) 7752–7759.

[27] S.W. Fetsko, P.T. Cummings, Brownian dynamics simulation of bead-spring chain models for dilute polymer solutions in elongational flow, J. Rheol. 39 (2) (1995) 285–299.

[28] T. Strick, J.-F. Allemand, V. Croquette, D. Bensimon, Twisting and stretching single DNA molecules, Prog. Biophys. Mol. Biol. 74 (2000) 115–140.

[29] C. Bustamante, J.F. Marko, E.D. Siggia, S. Smith, Entropic elasticity of λ-phage DNA, Science 265 (5178) (1994) 1599–1600.

[30] F. Johansen, J.P. Jacobson, 1H NMR studies of the bis-intercalation of a homodimeric oxazole yellow dye in DNA oligonucleotides, J. Biomol. Struct. Dyn. 16 (2) (1998) 205–222.

[31] B. Ladoux, P.S. Doyle, Stretching tethered DNA chains in shear flow, Europhys. Lett. 52 (5) (2000) 511–517.

[32] C.M. Bender, S.A. Orszag, Advanced Mathematical Methods for Scientists and Engineers: Asymptotic Methods and Perturbation Theory, Springer, New York, 1999.

[33] D. Keller, D. Swigon, C. Bustamante, Relating single-molecule measurements to thermodynamics, Biophys. J. 84 (2) (2003) 733–738.

[34] A. Dhar, D. Chaudhuri, Triple minima in free energy of semiflexible polymers, Phys. Rev. Lett. 89 (6) (2002) 065502.

[35] J. Samuel, S. Sinha, Elasticity of semiflexible polymers, Phys. Rev. E 66 (2002) 050801.